



A physical–biochemical model of plankton productivity and nitrogen cycling in the Black Sea

Temel Oguz^{a,*}, Hugh W. Ducklow^b, Paola Malanotte-Rizzoli^c,
James W. Murray^d, E.A. Shushkina^e, V.I. Vedernikov^e,
Umit Unluata^a

^a *Institute of Marine Sciences, Middle East Technical University, Erdemli, Icel, Turkey*

^b *The College of William and Mary, Virginia Institute of Marine Sciences, Gloucester Point, VA, USA*

^c *Department of Earth, Atmospheric and Planetary Sciences, Massachusetts Institute of Technology, Cambridge, MA, USA*

^d *School of Oceanography, University of Washington, Box 357940, Seattle, WA, USA*

^e *P.P. Shirshov Institute of Oceanology, Russian Academy of Sciences, Moscow, Russia*

Received: 8 July 1997; received in revised form 10 February 1998; accepted: 27 March 1998

Abstract

A one-dimensional, vertically resolved, physical–biochemical upper ocean model is utilized to study plankton productivity and nitrogen cycling in the central Black Sea region characterized by cyclonic gyral circulation. The model is an extension of the one given by Oguz et al. (1996, *J. Geophys. Res.* 101, 16585–16599) with identical physical characteristics but incorporating a multi-component plankton structure in its biological module. Phytoplankton are represented by two groups, typifying diatoms and flagellates. Zooplankton are also separated into two groups: microzooplankton (nominally <200 μm) and mesozooplankton (0.2–2 mm). The other components of the biochemical model are detritus and nitrogen in the forms of nitrate and ammonium. The model incorporates, in addition to plankton productivity and organic matter generation, nitrogen remineralization (ammonification) and ammonium oxidation (nitrification) in the water column. Numerical simulations are described and compared with the available data from the central Black Sea. The main seasonal and vertical characteristics of phytoplankton and nutrient dynamics inferred from observations appear to be reasonably well represented by the model. Fractionation of the biotic community structure is shown to lead to increased plankton productivity during the summer period following the diatom-based early spring (March) bloom. The annual nitrogen budget for the euphotic zone reveals the substantial role of recycled nitrogen in the surface waters of the Black Sea. © 1999 Elsevier Science Ltd. All rights reserved.

* Corresponding author. Tel.: 90 324 521 2406; fax: 90 324 521 2327; e-mail: oguz@deniz.ims.metu.edu.tr

1. Introduction

The Black Sea is known as one of the best examples of highly stratified marginal seas. This two layer stratified system is accompanied by a distinct biochemical structure characterized by complete anoxia of the sub-pycnocline waters and their separation from the oxygenated surface waters through a transition zone, called the Suboxic Layer (SOL) (Murray et al., 1989). The oxygenated surface layer comprises an euphotic zone of about 40–50 m underlain by an oxycline/nutricline zone of 20–30 m. The suboxic layer has a thickness of about 20–40 m and contains no measurable oxygen or sulphide.

The Black Sea contains an efficient mechanism of nitrogen cycling. About 90% of the particulate organic material sinking from the euphotic zone is mineralized in the euphotic zone and oxycline/nutricline zone below. The nutrients regenerated are then resupplied back to the surface waters, where they are depleted eventually by biological utilization (e.g. spring phytoplankton bloom). Only a small fraction of the particulate matter sinks to the deeper, anoxic zone (Lebedeva and Vostokov, 1984; Karl and Knauer, 1991). In the anoxic layer, particulate flux may give rise to chemosynthetic production, which amounts to approximately 10% of the photosynthetic production (Deuser, 1971; Brewer and Murray, 1973). As compared with basins rich in oxygen, a distinguishing feature of the Black Sea is limitation of primary production by subsurface nitrogen supply due to extensive nitrate consumption by denitrification in the subsurface waters. The deep anoxic water in the Black Sea contains no measurable nitrate but constitutes a large pool of reduced nitrogen in the forms of ammonium and dissolved organic nitrogen. The existing data indicate that ammonium transported upwards is oxidized immediately near the suboxic-anoxic interface zone by nitrate and MnO_2 (Murray et al., 1997) and lost to the atmosphere in the form of nitrogen gas. The anoxic layer thus does not appear to be a source of dissolved inorganic nitrate to the euphotic zone in the Black Sea.

The Black Sea has a major diatom bloom during March (Sorokin, 1983; Vinogradov, 1992; Vedernikov and Demidov, 1993). A second bloom occurs sometime during autumn. Two or more additional phytoplankton peaks, mainly of coccolithophorids and flagellates, are usually observed during late spring and summer (Bologa, 1986). *Emiliana huxleyi* blooms occurring in the months of June and July are evident in the CZCS imagery (Sur et al., 1996).

The early spring bloom is the most robust feature of the yearly phytoplankton structure and is present in every data set (see Koblenz-Mishke, 1970; Sorokin, 1983; Lebedeva and Vostokov, 1984; Vedernikov and Demidov, 1993). Formation and timing of summer blooms, on the other hand, seem to be much more sensitive to local conditions and exhibit considerable regional and interannual variability (Vinogradov, 1992; Vedernikov and Demidov, 1993; Sur et al., 1996).

As a part of our ongoing interdisciplinary modeling efforts, we recently constructed a one-dimensional nitrogen-based, vertically resolved, coupled physical–biological model of the lower trophic level to examine the first order physical and biological processes controlling the seasonal cycle of the plankton productivity in the surface waters of the Black Sea (Oguz et al., 1996, 1997). The biological part of the model was

kept quite simple, including only single phytoplankton and herbivore zooplankton groups (1P1Z), detritus, nitrate and ammonium, which form the “minimum critical set” (GLOBEC, 1995). The model was applied for conditions appropriate to the central Black Sea, which possesses simpler ecosystem behavior than do the highly complex western shelf and Rim Current frontal zones. This model had a reasonable success in reproducing monthly variations of the upper layer water column stratification characteristics. It demonstrated the crucial role of mixed layer dynamics during convective overturning events, which are missing in most ecosystem models. The biological component of this coupled model was able to simulate the spring and fall blooms and the summer subsurface chlorophyll maximum layer. This simple model was useful for examining the basic physical and biological processes controlling the seasonal cycle of plankton productivity in the Black Sea.

One drawback of the simplified 1P1Z ecosystem model was underestimation of the summer production. The summer subsurface chlorophyll concentrations were found to be somewhat lower than observed values. The limited capability of 1P1Z models in predicting summer chlorophyll values was noted earlier by Sarmiento et al. (1993) in their North Atlantic model. Armstrong (1994) pointed out that multiple prey–multiple predator models can alleviate the limitations imposed by 1P1Z approaches and, as in the North Atlantic case, may generate increased chlorophyll concentrations comparable with observations. In the present paper, we introduce two phytoplankton species groups, typifying diatoms and flagellates, and two zooplankton groups (micro- and mesozooplankton). Then we show how this slightly more complex representation of plankton food web structure leads to enhanced production during late spring and summer in the Black Sea model. In view of growing recognition of its importance, we also include a simple representation of ammonium oxidation (nitrification).

In more general terms our objective, given the idealized external conditions and idealized trophic-dynamic description of the system, is to investigate how successfully we can simulate the main features of nitrogen cycling and the yearly evolution of plankton production in the central Black Sea.

2. Model description

The model consists of physical and biochemical modules connected through the Mellor-Yamada level 2.5 turbulence module used for calculating vertical eddy fluxes. The details of the physical and turbulent components of the coupled model have been described previously (Oguz et al., 1996). We therefore present here only the basic elements of the biochemical model, whose main features generally follow Ducklow and Fasham (1992), excluding bacterial processes.

2.1. Governing equations

Nitrogen cycling and plankton dynamics in the upper layer of the Black Sea are modeled using two groups of phytoplankton and of herbivorous/omnivorous

zooplankton, together with labile particulate detritus D, nitrate NO_3 and ammonium NH_4 . The two phytoplankton groups typify diatoms and flagellates, and the two herbivore groups are microzooplankton Z_s (nominally $< 200 \mu\text{m}$) and mesozooplankton Z_ℓ (0.2–2 mm). The microzooplankton compartment includes heterotrophic flagellates, ciliates and juvenile copepods. The mesozooplankton compartment essentially represents adult copepods. Particulate organic detritus is assumed to be converted directly to ammonium without explicitly considering the microbial loop mediating the particle decomposition process.

The local temporal variations of all biological variables are expressed by equations of the general form

$$\frac{\partial F}{\partial t} + w_d \frac{\partial F}{\partial z} = \frac{\partial}{\partial z} \left[(K_b + v_b) \frac{\partial F}{\partial z} \right] + \mathfrak{R}_F \quad (1)$$

where t is time, z is the vertical coordinate, ∂ denotes partial differentiation, w_d signifies the sinking velocity, K_b is the vertical turbulent diffusion coefficient, and v_b is its background value. Here, we consider downward sinking only of detrital material; w_d is thus set to zero except in the detritus equation. The interaction term, \mathfrak{R}_F , is expressed as a balance of biological sources and sinks for each of the variables described below. A schematic representation of the biological processes included in the model is shown in Fig. 1a.

2.1.1. Phytoplankton

Variations of diatom (P_d) and flagellate (P_f) stocks are governed by a balance between growth (primary production) and losses due to herbivore grazing and physiological mortality. The effects of respiration and phytoplankton excretion are included in the latter loss term, since our model does not include a microbial loop component at present.

$$\text{Flagellates: } \mathfrak{R}_{P_f} = \sigma_f \Phi P_f - G_s(P_f) Z_s - G_\ell(P_f) Z_\ell - m_f P_f \quad (2)$$

$$\text{Diatoms: } \mathfrak{R}_{P_d} = \sigma_d \Phi P_d - G_s(P_d) Z_s - G_\ell(P_d) Z_\ell - m_d P_d \quad (3)$$

The phytoplankton growth is modeled as the product of the maximum specific growth rate σ , the overall limitation function Φ and the phytoplankton concentration P . The overall limiting factor on the maximum growth rate is defined as the minimum of the light and nutrient limitation terms:

$$\Phi = \min[\alpha(I), \beta_t(\text{NO}_3, \text{NH}_4)] \quad (4)$$

where $\alpha(I)$ is the light limitation function, $\beta_t(\text{NO}_3, \text{NH}_4)$ is the sum of ammonium and nitrate limitation functions represented, respectively, by $\beta_a(\text{NH}_4)$ and $\beta_n(\text{NO}_3)$. They are expressed by standard Michaelis–Menten uptake formulations (see Oguz et al., 1996). For simplicity, we ignore the difference in the photosynthetic and nutrient uptake abilities of diatoms and flagellates. The temperature control on the phytoplankton growth is also neglected. This is justified in the Black Sea by the fact that both

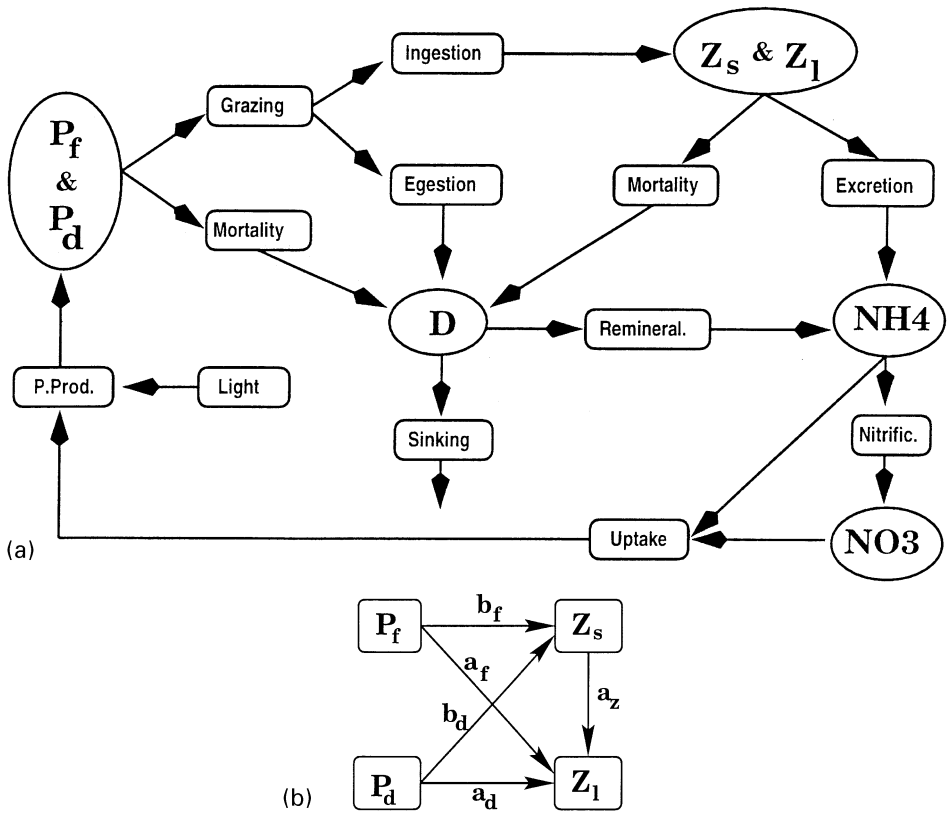


Fig. 1. (a) A schematic diagram showing the biological processes and interactions included in the model. (b) The trophic interactions between different plankton groups and food preference coefficients considered in the model.

early spring (typically in March) surface bloom and summer subsurface production below the seasonal thermocline occur at fairly uniform water temperatures around 7–10°C. We also exclude the role of silicate on the diatom blooms. Nitrate has been considered here as the single limiting nutrient for the central Black Sea conditions.

The light limitation is parameterized according to Jassby and Platt (1976) by

$$\alpha(I) = \tanh[aI(z, t)] \tag{5}$$

$$I(z, t) = I_s \exp[-(k_w + k_c P)z] \tag{6}$$

where a denotes the photosynthetic quantum efficiency parameter controlling the slope of $\alpha(I)$ versus the irradiance curve at low values of the photosynthetically active irradiance (PAR). I_s denotes the surface intensity of the PAR, taken as half of the climatological incoming solar radiation from the data given in Table 2 in Oguz et al. (1996). k_w is the extinction coefficient of the sea water, and k_c is the phytoplankton

self-shading coefficient. In the above formulation, both of these light attenuation coefficients are taken to be constant with depth.

2.1.2. Zooplankton

Changes in the microzooplankton (Z_s) and mesozooplankton (Z_ℓ) biomasses are controlled by ingestion, grazing, mortality and excretion.

$$\text{Microzooplankton: } \mathfrak{R}_{Z_s} = \gamma_s[G_s(P_f) + G_s(P_d)]Z_s - G_\ell(Z_s)Z_\ell - \mu_s Z_s - \lambda_s Z_s^2 \quad (7)$$

$$\text{Mesozooplankton: } \mathfrak{R}_{Z_\ell} = \gamma_\ell[G_\ell(P_f) + G_\ell(P_d) + G_\ell(Z_s)]Z_\ell - \mu_\ell Z_\ell - \lambda_\ell Z_\ell^2 \quad (8)$$

where μ_ℓ and μ_s are excretion rates, λ_ℓ and λ_s are mortality rates, and γ_ℓ and γ_s are the assimilation coefficients. In Eqs. (7) and (8), the mortality terms are expressed in the quadratic form as suggested by Steele and Henderson (1992). The role of other functional forms of the mortality (e.g. linear, hyperbolic) on the annual plankton variations are also investigated in this paper (see Section 4.8). Grazing is represented by the Michaelis–Menten relation and considers the food preferences, diatoms vs flagellates, of the two zooplankton groups. Using measures of zooplankton food preferences shown in Fig. 1b, we define total food available for each zooplankton group as

$$F_s = b_f P_f + b_d P_d \quad \text{and} \quad F_\ell = a_f P_f + a_d P_d + a_z Z_s. \quad (9)$$

The grazing rates of micro and mesozooplankton on flagellates are then defined by

$$G_s(P_f) = r_{gs} \frac{b_f P_f}{R_g + F_s} \quad \text{and} \quad G_\ell(P_f) = r_{g\ell} \frac{a_f P_f}{R_g + F_\ell}. \quad (10)$$

Similarly, the grazing rates of the two zooplankton groups on diatoms are

$$G_s(P_d) = r_{gs} \frac{b_d P_d}{R_g + F_s} \quad \text{and} \quad G_\ell(P_d) = r_{g\ell} \frac{a_d P_d}{R_g + F_\ell} \quad (11)$$

and a similar expression is applied for the grazing of mesozooplankton on the microzooplankton group. In Eqs. (10) and (11), r_{gs} and $r_{g\ell}$ denote the maximum specific grazing rates, and R_g is the half saturation ratio. As may be noted from Eqs. (7) and (8), zooplankton groups are assumed to assimilate uniform, constant fractions (represented by γ_ℓ and γ_s) of their ingestion.

Fasham et al. (1990) argued that the coefficients of food preferences should be expressed as functions of the relative prey densities (see Appendix A in Fasham et al., 1990). This approach seems to be more plausible than our specification of constant coefficients above, but it may introduce an additional complexity to the model due to the depth and time dependence of the coefficients. This point will be further discussed in Section 4.7.

2.1.3. Detritus

Fecal pellets, constituting the unassimilated part of ingested food, and phytoplankton and zooplankton mortalities, are the sources of detritus. As the detrital material

sinks with a speed w_d , it is transformed into ammonium with a rate εD . Here, for simplicity, the model considers only one class of detritus, which is produced by both phytoplankton and zooplankton groups, and sinks with a single settling velocity w_d . A more realistic approach would be to consider different size classes of detritus produced separately from different plankton groups and sinking with different settling velocities (cf. Prunet et al., 1996).

$$\begin{aligned} \mathcal{R}_D = & (1 - \gamma_s) [G_s(P_f) + G_s(P_d)]Z_s + (1 - \gamma_\ell) [G_\ell(P_f) + G_\ell(P_d) + G_\ell(Z_s)]Z_\ell \\ & + m_f P_f + m_d P_d + \lambda_s Z_s^2 + \lambda_\ell Z_\ell^2 - \varepsilon D. \end{aligned} \tag{12}$$

2.1.4. Nutrients

Two forms of nitrogen (ammonium and nitrate) support phytoplankton growth. As we shall discuss in Section 4, however, their roles in supporting regenerated and new production are not distinct, since the model includes nitrification. Excretion by two zooplankton groups and remineralization of detritus supply recycled ammonium. The losses are ammonium uptake during phytoplankton production and its oxidation to nitrate. The intermediate step of nitrite production was included in the nitrification process in our preliminary experiments but taken out later, since it had no distinguishable contribution to the euphotic zone budget. The data (cf. Codispoti et al., 1991; Basturk et al., 1994) indicate that nitrite concentrations in the euphotic zone are always smaller than those of other forms of nitrogen.

$$\text{Ammonium: } \mathcal{R}_{\text{NH}_4} = -\Phi \left(\frac{\beta_a}{\beta_t} \right) (\sigma_f P_f + \sigma_d P_d) - \Omega_a(z) \text{NH}_4 + \varepsilon D + \mu_s Z_s + \mu_\ell Z_\ell. \tag{13}$$

The nitrate equation consists of a source from ammonium oxidation and a loss by nitrate uptake, which also includes the ammonium inhibition effect (Oguz et al., 1996).

$$\text{Nitrate: } \mathcal{R}_{\text{NO}_3} = -\Phi \left(\frac{\beta_n}{\beta_t} \right) (\sigma_f P_f + \sigma_d P_d) + \Omega_a(z) \text{NH}_4. \tag{14}$$

2.2. Boundary conditions

All turbulent fluxes are set to zero at the surface and bottom boundaries of the biochemical model. Thus, we take

$$\left[(K_b + v_b) \frac{\partial F}{\partial z} \right] = 0 \quad \text{at } z = 0 \quad \text{and } z = -h_b. \tag{15}$$

In addition, the detritus equation includes

$$w_d D = 0 \quad \text{at } z = 0 \quad \text{and} \quad \frac{\partial (w_d D)}{\partial z} = 0 \quad \text{at } z = -h_b. \tag{16}$$

The bottom boundary of the model, h_b , is taken at a depth of 150 m, which is situated well below the level of active remineralization and nitrification taking place in the model. This choice of water column depth, together with the choice of a relatively low settling speed of 2.0 m d^{-1} , implies that our detrital pool, formed essentially by small particles, is remineralized completely within the water column without any export flux of particulate matter from the system. We thus consider that larger particles with much higher sinking rates are lost immediately and do not take part in the nitrogen recycling process in the upper layer. As shown in Oguz et al. (1996) and reported by similar models of plankton productivity (e.g. Jamart et al., 1977; Stigebrandt and Wulff, 1987; Sarmiento et al., 1993; Loukos et al., 1997), the detritus sinking velocity is in fact one of the critical model parameters, whose choice may considerably alter the annual plankton structure.

Within the framework of a one dimensional model, the assumption of complete remineralization is a fairly realistic approximation. The sediment trap observations suggest remineralization of more than 90% of the particulate organic matter within the upper layer ($\sim 100 \text{ m}$) of the Black Sea (Karl and Knauer, 1991). The advantage of a 100% remineralization assumption is to have a fully conservative system (note that $\sum \mathcal{R}_F = 0$ in our model), which therefore does not require us to deal with nitrate-based source/sink fluxes at the lower boundary of the model. In fact, specification of nitrate flux at the lower boundary, to compensate the fecal pellet loss, is not a straight forward issue in a one dimensional Black Sea ecosystem model. Contrary to the presence of deep nitrate pools in the Atlantic or Pacific, Black Sea subsurface waters consist of a deep ammonium pool, without any nitrate below about 100 m depth (see Section 3.2). This implies that organic matter loss to the deep waters should therefore be compensated by lateral nitrate fluxes, mostly originating from the Danube River discharge. On the other hand, the deep ammonium pool does not act as a nitrogen source to the euphotic zone in the Black Sea, because the ammonium transported upwards is consumed by its oxidation near the oxic/anoxic interface (see Fig. 5d). In reality, the bottom boundary of the euphotic zone is a very complicated region of redox processes in the Black Sea. A key feature is the suboxic zone, where the total fixed nitrogen goes to a strong minimum, suggesting conversion to nitrogen gas (Murray et al., 1999). Near the anoxic interface, ammonium is oxidized with MnO_2 and converted to nitrogen gas. These processes are too complicated to include in this model and beyond the scope of the present work.

2.3. Initial conditions and numerical procedure

The physical model is initialized by stably stratified upper ocean temperature and salinity profiles representative of the autumn conditions for the interior part of the sea. It is forced by the monthly climatological wind stress and surface thermal fluxes (see Table 2 in Oguz et al., 1996), whereas no-stress, no-heat and no-salt flux conditions are specified at the bottom. The biochemical model is initialized by a vertically uniform nitrate concentration of 4 mmol/m^3 within the euphotic and nitracline zones. The nitrate concentrations are set to zero below 75 m, corresponding roughly to oxygen depleted waters of the central Black Sea. Other state variables of the

biochemical model are initialized with small constant values over the water column to allow positive growth and utilization. Once the model equations are integrated ahead in time, the internal dynamics (i.e. plankton productivity, nitrogen cycling and vertical diffusion) establish realistic structures of the nitrate and other variables after a few years of transient adjustment.

The details of the numerical solution procedure are described in Oguz et al. (1996). A total of 50 vertical levels is used to resolve the 150 m thick water column. A time step of 10 min is used in the numerical integration of the system of equations. First, the physical model is integrated for five years to achieve a yearly cycle of the upper layer physical structure. Using these results, the biochemical model is then integrated for four years, which is sufficient to complete its transient adjustment from the initial conditions.

3. Observations

3.1. *Chlorophyll-a*

A series of vertical profiles of chlorophyll-*a* concentrations is shown in Fig. 2. These profiles are selected from measurements performed within the interior of the sea during the past decade on eight different cruises by the Shirshov Institute of Oceanology, Moscow (Vedernikov and Demidov, 1993). The first four profiles of March 1988 provide a clear indication of the spring bloom during the first half of the month. The profiles are homogeneous within the upper 40 m of the water column with typical concentrations of 2 mg m^{-3} . The bloom declines gradually during the second half of March to about 0.5 mg m^{-3} at the end of the month. The April and May data reveal surface mixed layer chlorophyll concentrations around $0.2\text{--}0.3 \text{ mg m}^{-3}$. A narrow subsurface chlorophyll maximum may also be traced at some stations. The thickness of this layer is less than 20 m, centered around 40 m. In May, peak concentrations do not exceed 0.5 mg m^{-3} .

An increase in subsurface chlorophyll concentrations is observed during June. The subsurface chlorophyll maximum reaches 1.0 mg m^{-3} near the base of the euphotic zone. The thickness and position of the subsurface maximum zone, however, vary regionally within the basin. This kind of enhanced subsurface chlorophyll signature seems to persist throughout the summer, as shown by the August 1989 data set. The October 1978 data suggest that the late summer-early autumn is a period in which the subsurface chlorophyll maximum layer is gradually eroded and narrowed. As implied by the data sets, this transitional period is followed by initiation of an autumn bloom episode towards the end of October. The November 1991 data set exhibits similar autumn bloom formation during the first half of November, with chlorophyll concentrations in excess of 1 mg m^{-3} in the 25 m thick surface mixed layer.

Interpretation of the chlorophyll data shown in Fig. 2 must consider interannual and regional variations. These merged observations indicate two distinct surface bloom episodes during March and November and increased subsurface production in

the summer months (June–August). Early October appears to be a transitional period of weak chlorophyll concentrations prior to the autumn bloom.

3.2. Phytoplankton and zooplankton

The yearly variations of the euphotic zone-integrated phytoplankton and zooplankton (micro- and meso-) biomasses are shown in Fig. 3. These distributions are formed using the data collected within the central Black Sea by the Shirshov Institute of Oceanology during seven cruises between 1978 and 1992. Because they are composites of different data sets, they can be used to infer only major signatures of the plankton system.

As in the case of the chlorophyll (Fig. 2), the phytoplankton data (Fig. 3a) reveal a strong bloom in early March, with the highest phytoplankton biomass of $\sim 7.0 \text{ gCm}^{-2}$ measured during 1991 survey. The data exhibit a decreasing trend

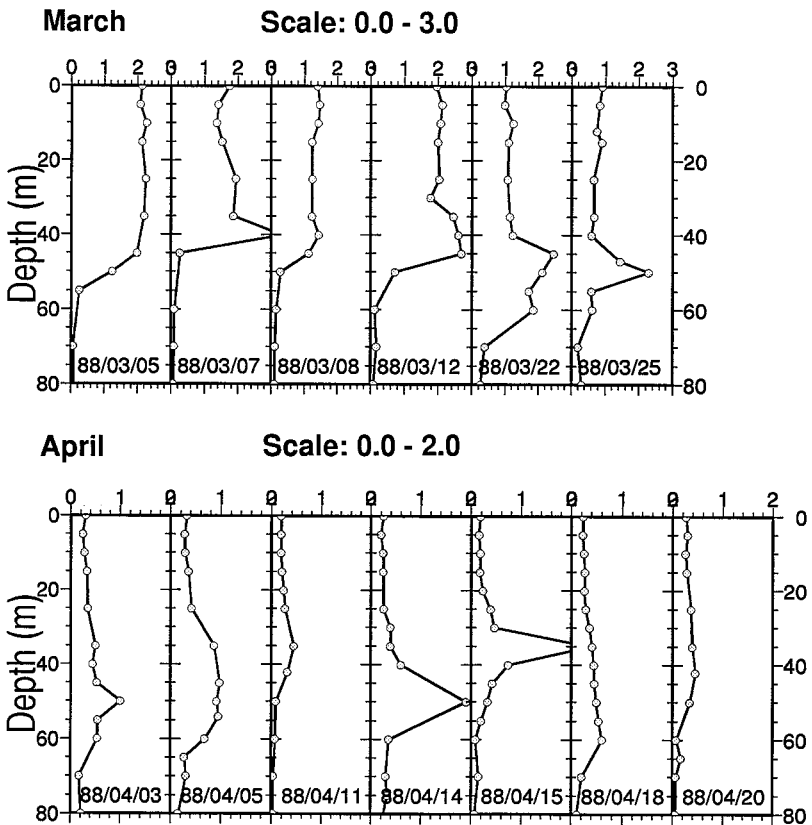


Fig. 2. Annual variations of the vertical chlorophyll-*a* (mg m^{-3}) structure derived from measurements carried out during 1978–1989 by Shirshov Institute of Oceanology, Moscow, and compiled by V.I. Vedernikov. The dates are shown for each profile in the form of three consecutive two digit numbers indicating the year, the month and the day of the measurements.

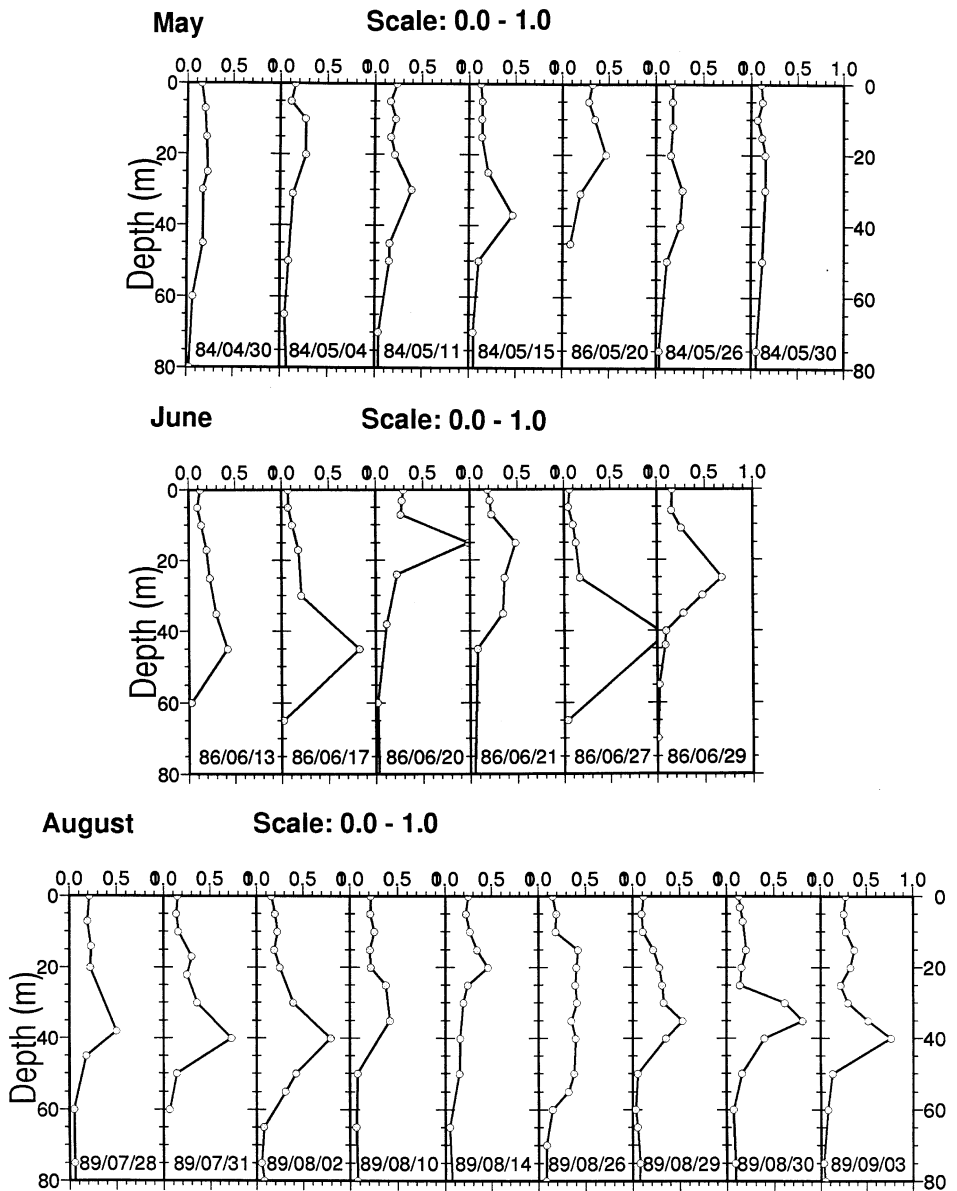


Fig. 2. (continued)

during late March–April, towards a minimum value of around 1.0 gC m^{-2} at the end of April. A secondary peak is observed in November, as inferred earlier from the chlorophyll data. The summer data, limited to the August–September period, suggest biomass values $\sim 2.0 \text{ gC m}^{-2}$.

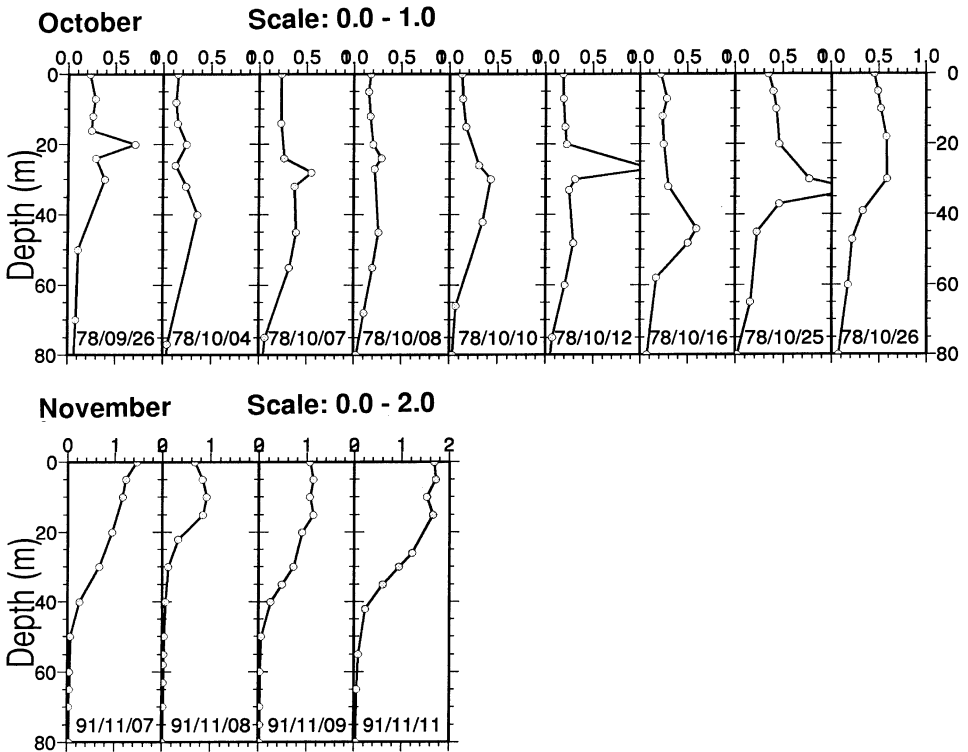


Fig. 2. (continued)

The yearly mesozooplankton structure (Fig. 3b) follows generally that of the phytoplankton. A major increase in the biomass occurs towards the end of March–mid-April, following the strongest phytoplankton bloom of the year. The peak biomass values are $\sim 2.0 \text{ gC m}^{-2}$ and reduced by half later during the summer. Because no measurements are available in the second half of November and December, the data do not provide a clear indication of autumn–early winter biomass increase following the autumn phytoplankton bloom. The microzooplankton, on the other hand, do not exhibit any appreciable seasonal variations. Their biomass remains typically below 0.5 gC m^{-2} throughout the year (Fig. 3c).

3.3. Nitrate

Examples of summer and winter nitrate profiles are shown in Fig. 4. The summer profiles, which are taken within the cyclonic gyre of the western basin, exhibit complete nitrate depletion within the upper 50 m, corresponding roughly to the euphotic zone. Nitrate then increases sharply to a maximum value of 8 mmol m^{-3} at 70–80 m through a sharp nitracline zone. It is quantified in the next section that

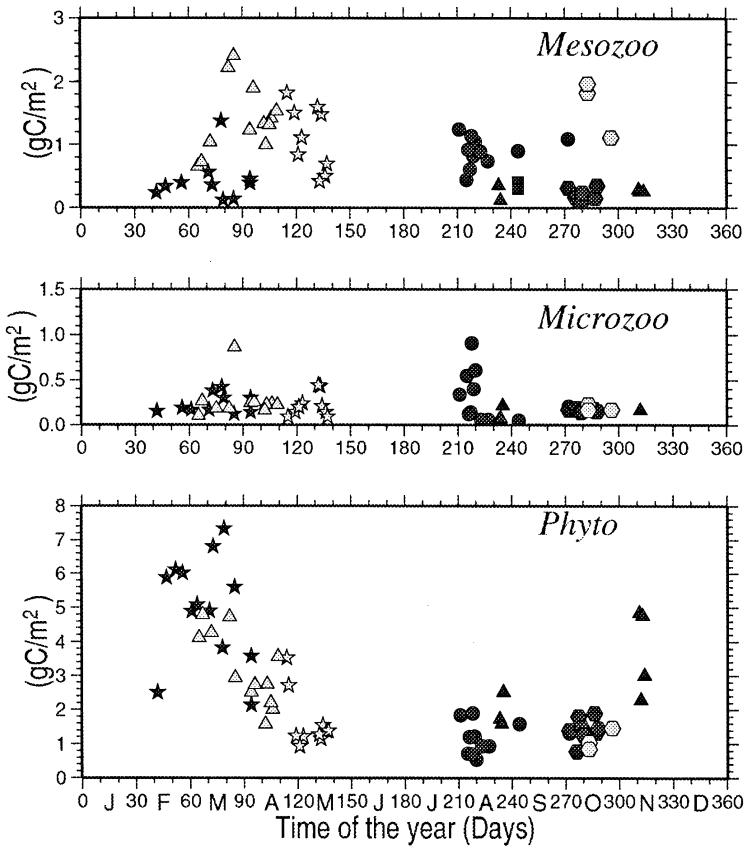


Fig. 3. A composite picture of the euphotic layer integrated (a) phytoplankton, (b) mesozooplankton, (c) microzooplankton distributions (in mgC m^{-2}) within a year compiled from different data sources (open hexagons, 1978; open stars, 1984; open triangles, 1988; solid circles, 1989; solid triangles and stars, 1991; solid hexagons, 1992).

formation of the nitracline through a sharp nitracline zone is a consequence of intense remineralization–nitrification processes.

The region below the nitrate peak is characterized by a sharp reduction in nitrate concentrations. In this oxygen-deficient part of the water column, organic matter degradation occurs via denitrification. In this process, bacteria utilize nitrate ions to oxidize organic matter from the surface layer. The nitrate is then reduced to nitrogen gas, with nitrite as an intermediate product. The nitrogen gas is eventually ventilated to the atmosphere. Denitrification continues until all the nitrate is consumed within the oxygen-deficient part of the water column. The lower limit of this zone coincides roughly with the onset of the H_2S layer. These processes, however, have not been included in the present work.

The winter nitrate profile reveals concentrations in excess of 2.0 mmol m^{-3} within the upper mixed layer of about 60 m. As we shall show in the next section, the

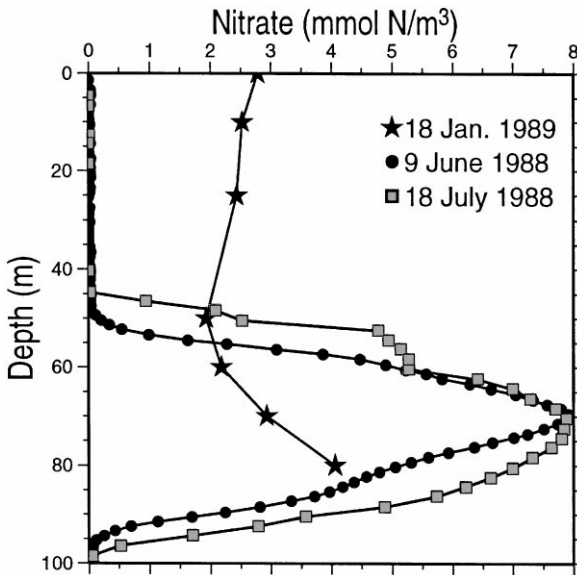


Fig. 4. Observed nitrate profiles in the upper water column of the Black Sea. Squares and circles signify the measurements of the R.V. Knorr at the center of the western gyre on 9 June and 18 July 1988. Stars show winter measurements performed at a station in the Rim Current frontal zone along the Turkish coast of the western Black Sea on 18 January 1989.

convective overturning process associated with the winter cooling is responsible for seasonal changes in the surface layer nitrate concentrations. The subsurface nitrate maximum of the observed winter profile in Fig. 4 is located at deeper levels than it is in the summer profiles. This is because this station is situated along the peripheral zone of the circulation system, which has an anticyclonic character. To our knowledge, winter nitrate measurements within the cyclonically dominated central basin are not available.

3.4. Ammonium

The vertical ammonium structure shown in Fig. 5a is characterized by low concentrations of less than 0.5 mmol m^{-3} within the upper 100 m of the water column, where it is converted continually to nitrate by nitrification and utilized by phytoplankton. The ammonium concentrations exhibit occasional peaks of about 0.5 mmol m^{-3} within the euphotic zone. It is shown in the next section that these peaks are related to summer phytoplankton production.

The ammonium concentration increases linearly below about 100 m depth, where the nitrate vanishes and the H_2S layer begins (Fig. 5b). It attains typically a value of 10 mmol m^{-3} at 150 m and 20 mmol m^{-3} at about 200 m depth. The deep ammonium pool has accumulated as a result of organic matter decomposition by sulfate

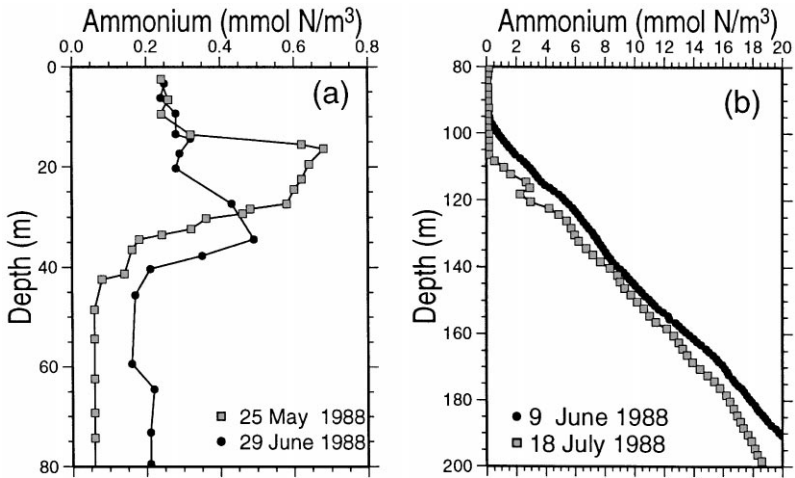


Fig. 5. (a). Ammonium profiles for the upper water column from the R.V. Knorr measurements at the center of the western gyre on 25 May and 29 June 1988. (b) Ammonium profiles from the R.V. Knorr measurements at the center of the western gyre, showing ammonium variations within the anoxic layer on 9 June and 18 July 1988.

reduction within the last 5000 years, since the Black Sea was converted into a two-layered stratified system (Boudreau and Leblond, 1989). The gradient of the ammonium profiles in the vicinity of the oxic-anoxic interface implies that no ammonium is supplied to the photic zone from the anoxic region.

As we have pointed out in the previous section, the present version of our Black Sea biogeochemical model includes neither denitrification (which is responsible for the formation of the lower nitracline) nor sulfate reduction (which leads to increases in the NH_4 concentrations in the anoxic layer). These simplifications are justifiable for our purpose of investigating the more intensive surface processes of plankton productivity.

4. Numerical simulations

4.1. Specification of parameters

The definition of parameters and their values are given in Table 1. Some of them are provided by existing observations and thus taken from the published literature on the Black Sea. Others are chosen from other seas having similar pelagic ecosystem and physical characteristics (see Oguz et al. 1996 for further discussion). The values of the photosynthesis quantum efficiency parameter a and the light extinction coefficient k_w are taken from our recent light measurements (Vidal, 1995). Their optimum values for the central Black Sea conditions are set to $a = 0.01(\text{W m}^{-2})^{-1}$ and $k_w = 0.08 \text{ m}^{-1}$. The self shading coefficient k_c is set to $0.07 \text{ m}^2(\text{mmol N})^{-1}$. Its value is, however,

Table 1
Model parameters used in the numerical experiments

Parameter	Definition	Value
a	Photosynthesis efficiency parameter	$0.01 \text{ m}^2 \text{ W}^{-1}$
k_w	Light extinction coefficient for PAR	0.08 m^{-1}
k_c	Phytoplankton self-shading coefficient	$0.07 \text{ m}^2 (\text{mmol N})^{-1}$
σ_d	Maximum growth rate for diatoms	1.5 d^{-1}
σ_f	Maximum growth rate for flagellates	1.0 d^{-1}
m_d	Diatom mortality rate	0.04 d^{-1}
m_f	Flagellate mortality rate	0.08 d^{-1}
r_i	Mesozooplankton maximum grazing rate	0.8 d^{-1}
r_s	Microzooplankton maximum grazing rate	1.2 d^{-1}
b_f, b_d	Food preferences of microzooplankton on flagellates and diatoms	0.7, 0.2
a_f, a_d, a_z	Food preferences of mesozooplankton on flagellates, diatoms and microzooplankton	0.3, 0.8, 0.7
λ_s	Mortality rate for microzooplankton	0.04 d^{-1}
λ_i	Mortality rate for mesozooplankton	0.08 d^{-1}
μ_i, μ_s	Zooplankton excretion rates	0.07 d^{-1}
γ_s, γ_i	Assimilation efficiencies	0.75
R_n	Half-saturation constant in nitrate uptake	$0.5 \text{ mmol N m}^{-3}$
R_a	Half-saturation constant in ammonium uptake	$0.2 \text{ mmol N m}^{-3}$
R_g	Half-saturation constant for zooplankton grazing	$0.5 \text{ mmol N m}^{-3}$
ψ	Ammonium inhibition parameter of nitrate uptake	$3 (\text{mmol N m}^{-3})^{-1}$
ε	Detritus decomposition rate	0.1 d^{-1}
w_s	Detrital sinkal rate	2.0 m d^{-1}
Ω_a	Nitrification rate	0.05 d^{-1}
ν_b	Background kinematic diffusivity for $z \leq 75 \text{ m}$	$1 \times 10^{-5} \text{ m}^2 \text{ s}^{-1}$
ν_b	Background kinematic diffusivity for $z > 75 \text{ m}$	$0.5 \times 10^{-5} \text{ m}^2 \text{ s}^{-1}$

found not to be critically important for altering the annual plankton distribution. The values of the half saturation constants are chosen from the literature (e.g. Fasham et al., 1990). They have typical values around $0.5 \text{ mmol N m}^{-3}$. For NO_3 we use $R_n = 0.5$ and for NH_4 , $R_a = 0.2$. Our sensitivity experiments indicate that the model response is not critically sensitive to their values.

The assimilation efficiencies (γ_s, γ_i) are taken to be 0.75, which is the most commonly cited value in the literature. The choices of the mortality and excretion rates depend on processes that are represented by these terms, but their typical values cited in the literature are around 0.05 d^{-1} . We use here phytoplankton mortality rates of $m_f = 0.08$ and $m_d = 0.04 \text{ d}^{-1}$. For zooplankton, we let the mortality rates be $\lambda_s = 0.04$ and $\lambda_i = 0.08$ and the excretion rates (μ_s, μ_i) 0.07 d^{-1} . Their particular choices are found to have secondary effects on the simulations. The values of maximum growth rates (σ_f, σ_d) and of the maximum grazing rates (r_s, r_i) are set to $(1.0, 1.5) \text{ d}^{-1}$ and $(1.2, 0.8) \text{ d}^{-1}$. In the model, each group of zooplankton can feed on two types of prey. We assume that the microzooplankton prey with greater efficiency on flagellates than on diatoms. We thus set the efficiency parameters to $b_f = 0.7$ and $b_d = 0.2$. Mesozooplankton are considered to prey more efficiently on diatoms ($a_d = 0.8$) than on flagellates

($a_f = 0.3$). Their food preference for microzooplankton is set to $a_z = 0.7$. These values were suggested by observations carried out by Shirshov Institute of Oceanology, Moscow, in the Black Sea.

The ammonium oxidation rate Ω_a is taken to be 0.05 d^{-1} above the depth of the 15.8 kg m^{-3} sigma- t level, which corresponds to the total oxygen depletion level in the central Black Sea. This value of Ω_a is estimated from measurements of Ward and Kilpatrick (1991). At deeper levels, where nitrification does not occur, its value is set to zero. The choice of constant Ω_a above the depth of the 15.8 kg m^{-3} sigma- t level is an idealization of its more realistic depth dependent representation according to the oxygen variations in the water column.

Within the euphotic layer and the nitracline, we assume a background vertical diffusion of $10^{-5} \text{ m}^2 \text{ s}^{-1}$. A smaller value of $0.5 \times 10^{-5} \text{ m}^2 \text{ s}^{-1}$ is used for the deeper part of the water column, where there is no biological activity, and corresponds to the permanent pycnocline with strong density differences ($\sim 3.0 \text{ kg m}^{-3}$) over an interval of 50 m. Using the empirical expression given by Gargett (1984), Lewis and Landing (1991) arrived at similar values of the vertical diffusivity in their Black Sea manganese cycling model.

A series of simulation experiments was carried out to classify these parameters according to sensitivity of major observed features to the choices of their values. In this way, we try to identify the most critical parameters and their range of values for predicting the annual cycle of plankton productivity consistent with available observations. Some examples of these sensitivity experiments will be described in the next sections.

4.2. Mixed layer structure

In Oguz et al. (1996), we described in some detail the ability of our physical model to simulate observed mixed layer temperature and salinity during the year using a fairly sophisticated turbulence parameterization. It was shown that seasonal cycles were correctly reproduced, with maximum sea surface temperature deviations of less than 0.5°C , and maximum mixed layer depth differences of 10 m. Here, we present some additional features of the mixed layer structure using depth-time distributions of the temperature and vertical eddy diffusivity during a perpetual year of the simulations (Fig. 6). The seasonal temperature variations (Fig. 6a) reveal a convectively formed 50 m deep mixed layer during winter, followed later by a shallow summer mixed layer (less than 20 m) and very sharp seasonal thermocline. The thicknesses as well as temperatures of both winter and summer structures agree well with the climatological data used in Oguz et al. (1996). The minimum value of simulated mixed layer temperature of 6.7°C is slightly higher than the typical coldest observed values of $5\text{--}6^\circ\text{C}$ and is due to the use of climatological, smoothed heat flux forcing in the model.

The seasonal evolution of the cold water mass situated immediately below the thermocline is as interesting as the seasonal mixed layer variability. During its winter formation period, it is colder than the underlying water mass by about 1.5°C . Following the onset of spring warming, the upper 20 m part of this cold water mass

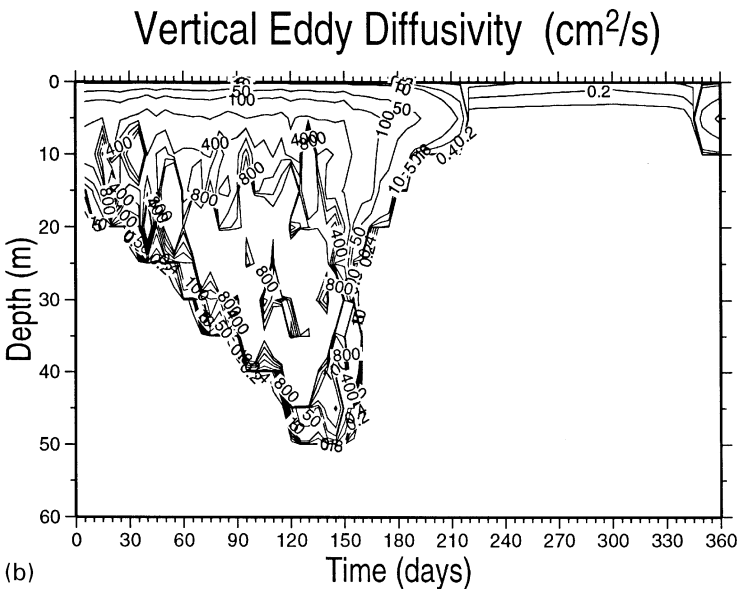
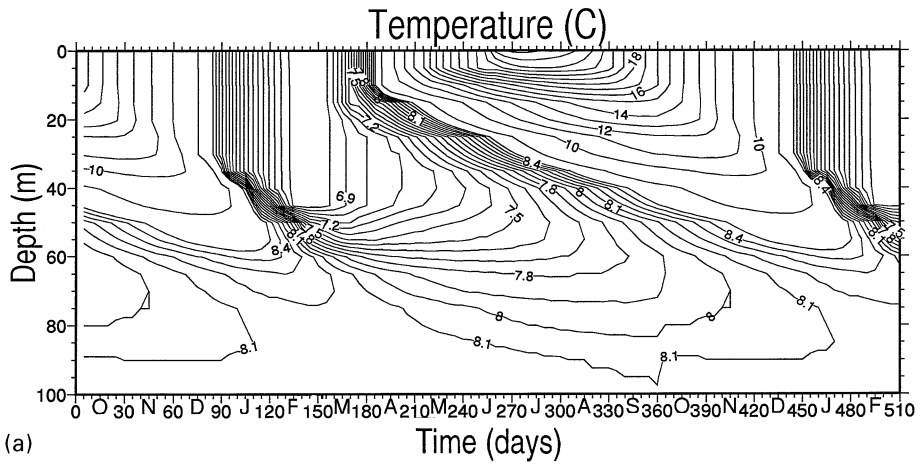


Fig. 6. (a) Yearly evolution of the upper layer temperature structure simulated by the model. (b) Annual variations of the vertical eddy diffusivity (in $\text{cm}^2 \text{s}^{-1}$) within the upper layer water column computed by the model.

gradually warms up and is isolated from the cold water core through a sharp seasonal thermocline. Below the thermocline, the cold water core subducts gradually towards slightly deeper levels during the rest of the season. In summer months, when the surface temperature becomes as high as 24–25°C, a temperature difference of about 18°C occurs within approximately 20 m below the shallow surface mixed layer. This very sharp seasonal thermocline plays a crucial role in the evolution of the summer phytoplankton structure.

October is a transitional period after which cooling of the surface waters gradually erodes the summer stratification. The end of December and beginning of January are times of weakest temperature stratification; the temperature of the entire upper layer varies around $8.5 \pm 0.5^\circ\text{C}$. This is followed by the next cycle of cold water mass formation during January–February. The formation and maintenance of the Cold Intermediate Water (CIW) are well-known features of the Black Sea thermohaline structure and discussed in many publications (cf. Oguz et al., 1992). It is advected by the basinwide cyclonic circulation around the basin, with its core centered at about 50 m depth. It has significant importance to the Black Sea fisheries.

Fig. 6b reveals great seasonal variability of the vertical mixing within the upper 50 m layer. Vertical eddy diffusivity is only a few $\text{cm}^2 \text{s}^{-1}$ above the thermocline during the summer season, decreasing to its background value of $0.1 \text{ cm}^2 \text{s}^{-1}$ below. This characterizes the detrainment phase of the mixed layer. Once the atmospheric cooling starts and the winds intensify in September, vertical mixing strengthens; the mixed layer entrains water from below and consequently deepens. Gradual development of this process is noted in Fig. 6b by a two order of magnitude increase in the value of the vertical eddy diffusivity in October. Late autumn and winter are the strongest cooling periods of the year, in which the vertical diffusivity exceeds values of $1000 \text{ cm}^2 \text{s}^{-1}$. The convective overturning process generates complete mixing and cools the uppermost 50 m of the water column. At the base of the mixed layer, on the other hand, the turbulence dies off quickly, and vertical eddy diffusivity decreases to its background value. This level of the vertical eddy diffusivity therefore provides a quantitative measure of the mixed layer depth.

4.3. *Summer phytoplankton production using a five-compartment model*

Before describing the phytoplankton bloom structures within a year using the seven compartment model, we first present here a solution of the summer phytoplankton concentration from the five-compartment model in which both phyto- and zooplankton are represented in aggregated form by single compartments. Using the parameter values of diatoms and mesozooplankton in Table 1, this simplified model produces the early spring bloom in March as well as the subsequent bloom supported primarily by regenerated production in April (Fig. 7). The entire summer season is, on the other hand, characterized by low subsurface chlorophyll concentrations of less than 0.15 mg m^{-3} . Oguz et al. (1996) showed that such low concentrations were the result of the grazing control. A similar situation will be shown for diatoms in the seven-compartment model here.

4.4. *Annual plankton and nitrogen cycles: a case study*

Using the set of parameters given in Table 1, we present below a case study for the simulation of annual plankton production and nitrogen cycling representative of interior Black Sea conditions, away from the shelf and the Rim Current frontal zone. The parameters used in this simulation experiment were adjusted within their

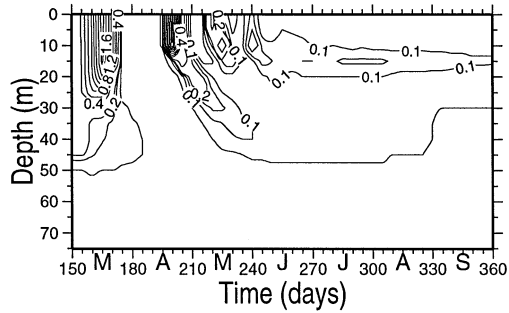


Fig. 7. Spring and summer phytoplankton distribution (mmol N m^{-3}) computed from five-compartment ecosystem model. The contour interval is 0.05 for phytoplankton biomass values less than $0.2 \text{ mmol N m}^{-3}$ and 0.2 for values greater than $0.2 \text{ mmol N m}^{-3}$.

uncertainty to be consistent with available Black Sea observations, some of which were described in Section 3.

4.4.1. Phytoplankton

Diatoms exhibit a major peak during the first half of March with maximum concentrations of about $2.3 \text{ mmol N m}^{-3}$ within the upper 30 m, decreasing towards the base of the mixed layer at 50 m (Fig. 8a). This early spring bloom is driven by new production associated with very strong entrainment of subsurface nitrate into the mixed layer prior to bloom formation (see Fig. 11). A shorter, secondary bloom event occurs during the second week of April. Contrary to the March bloom, it is related to ammonium-based regenerated production (Fig. 12) right after the March bloom. In summer below the shallow surface mixed layer, relatively weak subsurface production yields diatom concentrations of $0.15 \text{ mmol N m}^{-3}$ near the base of the euphotic zone. The development of larger subsurface summer concentrations is not possible because of mesozooplankton grazing pressure on the diatom cells, as in the case of the five-compartment model.

Flagellates exhibit a considerably different annual distribution (Fig. 8b). They have an extended bloom period during the late spring and summer below the mixed layer with the highest concentrations of $0.6 \text{ mmol N m}^{-3}$ taking place around 25–30 m depth during June. The subsurface phytoplankton production is eventually combined with the surface production during November, when vertical mixing entrains sufficient nitrate from the subsurface levels. This fall bloom has maximum concentrations of $0.35 \text{ mmol N m}^{-3}$. These features of the annual phytoplankton distribution are further shown by the depth-integrated stocks in Fig. 9.

4.4.2. Zooplankton

Because of strong grazing control by mesozooplankton (Z_m), microzooplankton (Z_s) stock remains low over the entire year (Fig. 9). The highest mesozooplankton concentrations reach $1.2 \text{ mmol N m}^{-3}$ (30 mmol N m^{-2}) during the last week of March following the major phytoplankton bloom in early March. After May, the

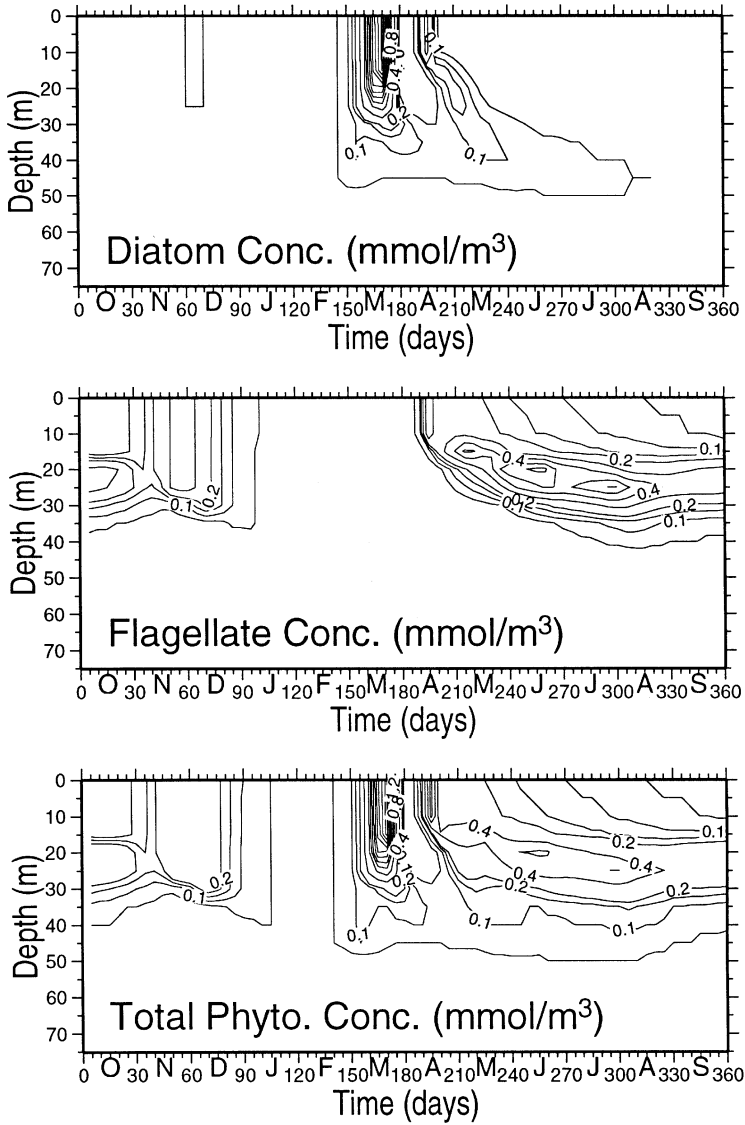


Fig. 8. The model derived annual distributions of (a) diatom biomass, (b) flagellate biomass, and (c) total phytoplankton biomass (mmol N m^{-3}) in the upper water column. The contour interval is 0.05 for phytoplankton biomass values less than $0.2 \text{ mmol N m}^{-3}$ and 0.2 for values greater than $0.2 \text{ mmol N m}^{-3}$.

mesozooplankton biomass in the euphotic zone declines gradually from 17 to 2 mmol N m^{-2} in November. A slight increase in mesozooplankton concentrations is observed in December following the autumn bloom event. In January and February the stock is at its minimum level (about 1 mmol N m^{-2}).

Depth Integrated Plankton Biomasses

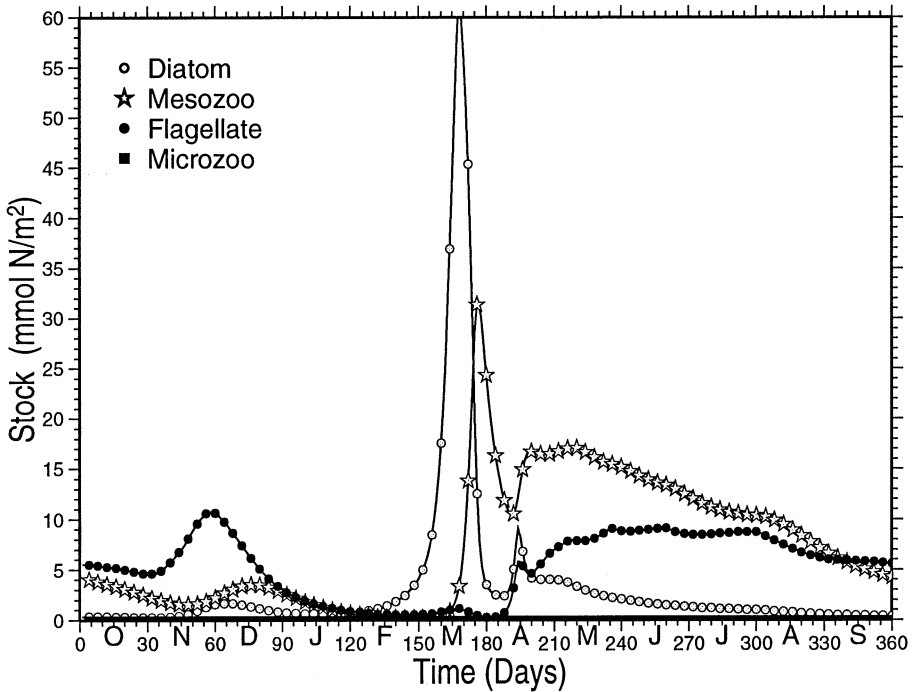


Fig. 9. Annual variations of the euphotic zone integrated plankton biomass (mmol N m^{-2}) computed by the model.

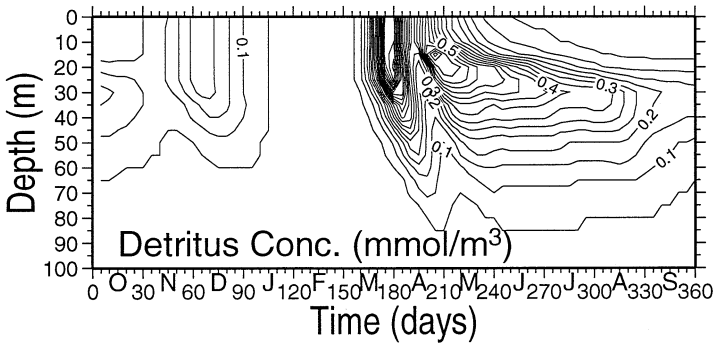


Fig. 10. The annual distribution of the detrital material (mmol N m^{-3}) in the upper water column computed by the model.

4.4.3. Detritus

The concentration of detritus (Fig. 10) is highest at $1.0 \text{ mmol N m}^{-3}$ right after the March bloom. Concentrations gradually decrease through the summer ($0.6 \text{ mmol N m}^{-3}$ in May–June and $0.2 \text{ mmol N m}^{-3}$ in August) due to mineralization

to ammonium. As expected from the temporal trends of phytoplankton and zooplankton biomass, there is no detritus present during winter. It has a surface signature only in March and accumulates below the seasonal thermocline to 100 m depth during the summer, which is 50 m above the base of the model. The detrital material is therefore completely remineralized within the water column without being exported to the deep anoxic layer through the base of the model, according to our assumption.

4.4.4. Nitrate

The nitrate profiles at selected times of the year are plotted in Fig. 11. The upper parts of the nitrate profiles are subject to considerable seasonal variability due to vertical mixing and uptake-remineralization-nitrification. Nitrate concentrations exhibit almost total depletion within the shallow surface mixed layer from May to November. The lack of sufficiently strong vertical mixing across the sharp seasonal thermocline allows consumption of the entire nitrate stock within the mixed layer during the summer. This layer is separated from waters having higher nitrate concentrations by a nitracline with a thickness of about 25 m. It is only after November, once the seasonal thermocline is eroded, that the surface layer begins to accumulate nitrate by entrainment from the nitrogen-rich subsurface waters. The entire convectively generated mixed layer thus attains a vertically uniform nitrate concentration up to $3.0 \text{ mmol N m}^{-3}$ during the winter period. The winter mixed layer is separated from the subsurface nitrate maximum zone by a stronger nitracline (10 m) centered approximately at 60 m. During the March–May, following the spring blooms, the layer

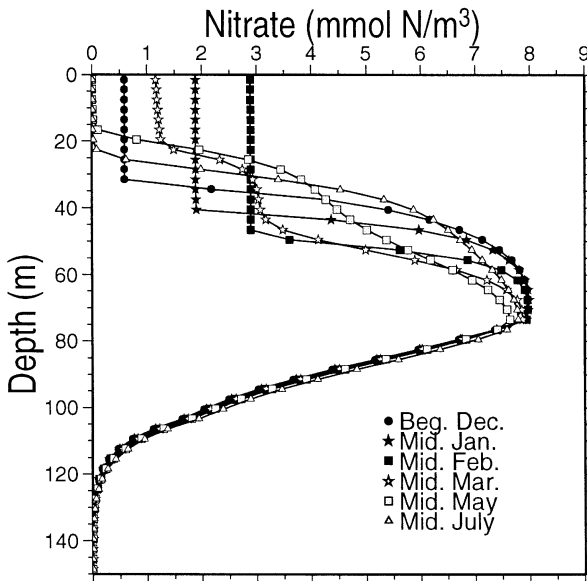


Fig. 11. The model derived nitrate profiles (mmol m^{-3}) at selected times of the year.

bounded by the seasonal thermocline and the nitracline becomes the biochemically active zone of continuous nitrification. Subsequently, this layer exhibits more gradual variations between the depleted surface waters and subsurface nitrate maximum.

The nitrate gradients change from 0.2 mmol m^{-4} during the summer period of shallowest mixed layer to 0.5 mmol m^{-4} during the winter period of deepest mixed layer formation. The persistent nitrate maximum occurs at approximately 75 m depth. Nitrate concentrations change from $7.6 \text{ mmol N m}^{-3}$ in spring to $8.1 \text{ mmol N m}^{-3}$ in winter. Below the nitrate peak, the profiles do not change seasonally and decrease to trace level concentrations at a depth of about 120 m. As mentioned earlier, the nitrate loss due to denitrification is not included in the model. The nitrate variations in this part of the water column result only from adjustment of the initial nitrate profile to its steady state form by vertical diffusion.

4.4.5. Ammonium

Vertical profiles of ammonium (NH_4) at different times of the year are shown in Fig. 12. The ammonium concentrations in the surface mixed layer increase gradually after December, as a result of its regeneration following the late autumn bloom and entrainment from subsurface levels. Ammonium concentrations reach about $0.25 \text{ mmol N m}^{-3}$ in mid-January, after which they decrease until the end of March on conversion to nitrate. Much higher surface ammonium concentrations (up to $1.0 \text{ mmol N m}^{-3}$) occur following the March bloom during late March–early April. Later in the spring and during the summer, ammonium within the mixed layer is consumed by phytoplankton and nitrifiers. The concentrations therefore decrease to

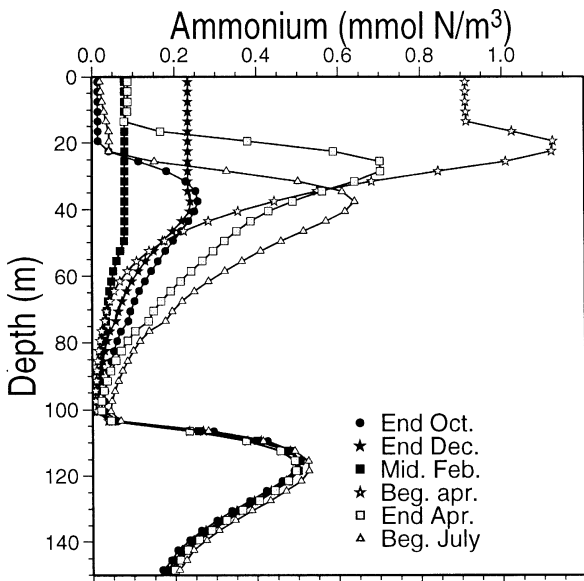


Fig. 12. The model derived ammonium profiles (mmol m^{-3}) at selected times of the year.

less than $0.05 \text{ mmol N m}^{-3}$ within the mixed layer. Below the mixed layer, the April–September period is characterized by relatively high ammonium concentrations on the order of $0.50 \text{ mmol N m}^{-3}$, which are again a consequence of subsurface production and remineralization-ammonification. Summer peaks at about 30–40 m depth imply the presence of maximum rate of ammonification within the euphotic zone, decreasing gradually downward in parallel with the decrease in the detritus concentrations.

The NH_4 concentrations are less than $0.1 \text{ mmol N m}^{-3}$ at the 100 m depth level. Ammonium profiles exhibit a sharp increase immediately below 100 m depth and then a gradual decrease towards the bottom boundary of the model. The sharp increase is due to the absence of nitrification at depths below 100 m. As we have pointed out earlier in Section 2.4, the ammonium oxidation rate was set to zero at depths below 100 m, defining roughly the boundary of the H_2S layer in the model. This sharp increase therefore provides a sign of ammonium accumulation within the H_2S layer. The ammonium dynamics shown here reflect the short-term biological processes addressed by this model. These profiles would take the alternate form shown in Fig. 5a if the model were designed for long-term integration in order to investigate the formation of ammonium pool. The reduction of concentrations towards the bottom is due to decreasing concentrations of detritus.

4.5. Model-data comparison

The model simulations given above are compared here with the observations presented in Section 3. For comparison of phytoplankton biomass with the chlorophyll-*a* observations, we use a conversion factor of $1 \text{ mmol N} \approx 1 \text{ mg Chl}$. This conversion factor considers an algal carbon to chlorophyll ratio of 100 and carbon to nitrogen ratio of 8.5, even though these numbers are subject to seasonal and regional variabilities over the Black Sea (Karl and Knauer, 1991; Burlakova et al., 1997; Coban, 1997). Total phytoplankton concentrations during the March bloom (Fig. 8c) are of the order of $2.0 \text{ mmol N m}^{-3}$ and agree well with the March chlorophyll data. The vertical uniformity is restricted to approximately 30 m depth in the model, compared to the observed 40 m. The vertical structure of the summer phytoplankton concentrations also agrees reasonably well with the data. The magnitude of subsurface chlorophyll maximum of $0.5 \text{ mmol N m}^{-3}$ produced by the model during June–August is consistent with typical observed chlorophyll peaks, although the data show higher values at some stations. The peaks in the model are confined to 20–30 m depths, whereas the observed peaks occur at slightly deeper levels of 30–40 m. The trend of slight reduction in the phytoplankton concentrations during September and early October is also indicated by the observations. The November bloom in the model has typical concentrations of $0.3 \text{ mmol N m}^{-3}$, whereas the data suggest much higher concentrations of the order of 1 mmol N m^{-3} .

Recent studies (Hurt and Armstrong, 1996; Doney et al., 1996) have shown how the inclusion of variable Chl:N ratios might provide a better matching of the model predictions of phytoplankton in nitrogen units to the Bermuda Time Series observations given in chlorophyll units. This was reported to provide a more reliable

prediction of the deep chlorophyll maximum, where Chl:N ratios may be elevated (relative to surface values) because of low light. Both Hurtt and Armstrong (1996) and Doney et al. (1996) used quite different values for the maximum chlorophyll-to-nitrogen ratio under light limited conditions. In nutrient limited conditions, they assigned different functional relationships to decrease this maximal value to a given background value. However, it is not clear how any one of these approaches might be adopted to the Black Sea conditions, given uncertainties on the values of several parameters that need to be specified. Therefore, in order not to introduce a further empiricism into the model, we adopt the constant chlorophyll-to-nitrogen conversion ratio of unity in the present study. This choice leads to a lower limit chlorophyll estimate by the model.

Taking 1 mmol N approximately equivalent to 0.1 gC, the depth integrated plankton biomasses shown in Fig. 9 are compared with the observations presented in Fig. 3. The peak phytoplankton biomass of 60 mmol N m^{-2} ($= 6.0 \text{ gC m}^{-2}$) during early March reflects typical measured biomasses in different parts of the basin at the same period of the year. The summer biomass values of about 10 mmol N m^{-2} simulated by the model also lie in the range of measured values ($0.5\text{--}1.5 \text{ gC m}^{-2}$). On the other hand, the computed values of phytoplankton biomass during the autumn bloom period are smaller than the observed values, as noted above.

The observations shown in Fig. 3 are inconclusive to support the presence of a secondary phytoplankton peak in April and subsequent short term variations in the mesozooplankton biomass. They are a consequence of nitrogen build up in the mesozooplankton pool during the initial bloom and its subsequent release a couple of weeks later. However, a slightly different parameter setting (e.g. a higher mortality rate for mesozooplankton) could yield a more rapid flux of nitrogen through the mesozooplankton pool and provide a more extended spring bloom without a discernable break.

There might be two reasons for underestimation of autumn bloom in the model. The first might be the absence of strong short term wind fluctuations in our climatological forcing. Such wind events might be very efficient for generating strong wind induced mixing during the late autumn (Klein and Coste, 1984). The second is related to the general limitation of the one dimensional models, which neglect the lateral advective transports of nutrients. A slight lateral input from the nitrate-rich peripheral zone by meanders of the Rim Current might strengthen the autumn bloom within the central basin.

The primary production computed by the model is compared with the values from a series of measurements during 1978–1991 reported by Vedernikov and Demidov (1993). On the basis of this data set, the euphotic layer integrated primary production distribution within the year was presented in Fig. 2c in Oguz et al. (1996). In the model, within the upper 50 m depth, it varies from a minimum value of about $100 \text{ mg C m}^{-2} \text{ d}^{-1}$ during winter (January–February) to a maximum of $1400 \text{ mg C m}^{-2} \text{ d}^{-1}$ at the time of the March bloom (Fig. 13). The latter value compares well with the measurements of 1000 to $1500 \text{ mg C m}^{-2} \text{ d}^{-1}$ at different stations within the central Black Sea and at different years. As shown by Fig. 13, it is associated with the nitrate-based new production, whereas two consecutive ones

Depth Integrated Primary Production

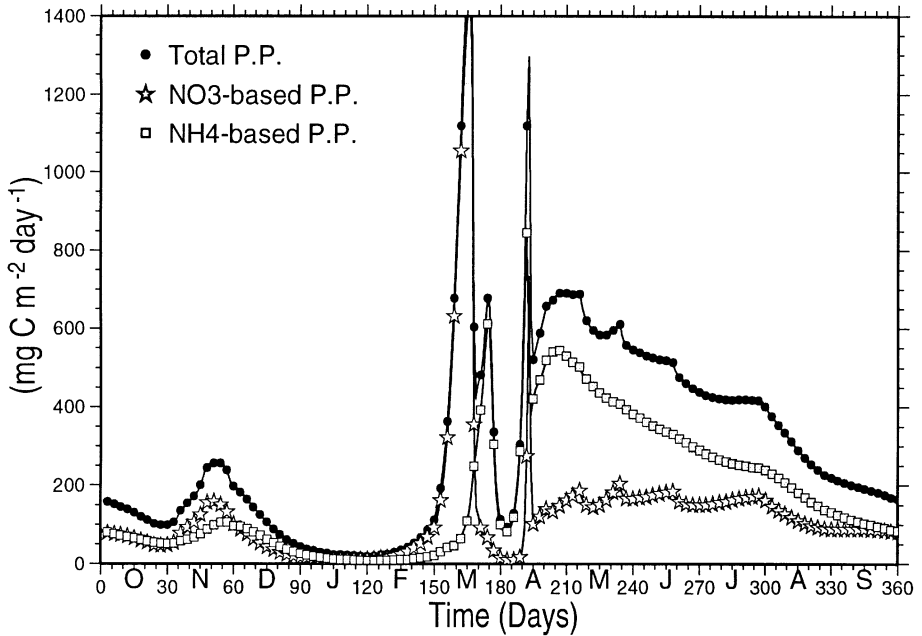


Fig. 13. Annual variations of the euphotic zone integrated nitrate-based, ammonium-based and total primary production ($\text{mg C m}^{-2} \text{d}^{-1}$) computed by the model.

during the second half of March ($\sim 700 \text{ mg C m}^{-2} \text{d}^{-1}$) and in April ($\sim 1000 \text{ mg C m}^{-2} \text{d}^{-1}$) are based on regenerated nitrogen. Typical measured values for this period are between 500 and $1000 \text{ mg C m}^{-2} \text{d}^{-1}$.

The total primary production decreases from late spring to autumn and is dominated by regenerated production (Fig. 13). Total production was around $600 \text{ mg C m}^{-2} \text{d}^{-1}$ during May, comparable to the value measured in situ during 1978 and 1988 (Vedernikov and Demidov, 1993). The computed primary production in June–July is characterized by values around $400\text{--}550 \text{ mg C m}^{-2} \text{d}^{-1}$, whereas the data suggest values from 250 to $500 \text{ mg C m}^{-2} \text{d}^{-1}$ in the same period. The autumn peak of the primary production is around $300 \text{ mg C m}^{-2} \text{d}^{-1}$, which is consistent with the value of $360 \text{ mg C m}^{-2} \text{d}^{-1}$ obtained as an average of measurements from all stations in the central Black Sea at the time of the autumn bloom (Vedernikov and Demidov, 1993). Furthermore, the annual primary production estimate of $67 \text{ g C m}^{-2} \text{yr}^{-1}$ from the model lies between the observed estimates of $40 \text{ g C m}^{-2} \text{yr}^{-1}$ (Finenko, 1979) and $90 \text{ g C m}^{-2} \text{yr}^{-1}$ (Sorokin, 1983) from the various measurements in the central part of the sea. This is almost half of the more recent estimate of $150 \text{ g C m}^{-2} \text{yr}^{-1}$ by Vedernikov and Demidov (1993). The latter value is, however misleading, since it is based on a multi-year composite data set, which includes more than one set of late winter–early spring bloom events that occurred on different days in

different years. The annual primary production rate therefore seems to be overestimated by these data.

We next compare the vertical nitrate and ammonium distributions with those from observations presented in Figs. 4 and 5a, b. Comparison of Fig. 4 and Fig. 11 indicates that the nitrate peak is reproduced at a similar depth level with similar concentration values. The upper nitracline zone exists in both figures with somewhat different structures. The nitrate depleted layer extends to 40 m in the observed profiles, whereas the summer profiles from the model have a depleted layer of only 20 m, followed by a more gradual slope of nitrate concentrations. The winter structure produced by the model is also supported by the observations of increased nitrate concentrations within the upper 60 m. The observed nitrate concentrations are, however, not as vertically homogeneous as they are in the model. The ammonium peaks simulated by the model during the summer months exist in the observations (Fig. 5a). In both observations and model results, the spring peak is stronger and located at a shallower level, compared to slightly deeper and weaker ammonium peaks in the summer months. The magnitude as well as the gradual reduction of the ammonium concentrations within the nitracline zone are consistent with the observed profiles.

4.6. *The dynamics of enhanced summer phytoplankton production*

The mechanisms triggering spring diatom bloom development have been described in Oguz et al. (1996, Section 4.2.3). Contrary to the classic concept of bloom formation at the times of vernal stratification, the diatom blooms were shown to depend on relative strength of the primary production and the vertical diffusion terms prior to the initiation of the bloom. These two terms have opposing contributions to the time rate of change term. When vertical diffusion overcomes the production, the bloom is delayed until the convection weakens. Then, as soon as the production term exceeds the vertical diffusion term (all other sink terms have negligible contribution), an exponential growth of diatoms takes place even when the mixed layer has not yet shallowed. This phenomenon may in fact be noticed in Fig. 8a, where the bloom initiation at day 155 (recall that day 1 corresponds to the beginning of October in the figures) coincides exactly with the onset of an order of magnitude decrease in the vertical eddy diffusivity shown in Fig. 6b. The March bloom is restricted to the upper 30 m, because a weaker light limitation below 30 m depth (see Fig. 9 in Oguz et al., 1996) prevents extension of the bloom to deeper levels.

Following the March bloom event, diatoms give rise to a secondary surface bloom during April and its subsurface extension during the first half of May (Figs. 8 and 9). The rest of the spring and the entire summer are characterized by extremely weak biological activity controlling the diatom stocks. As shown in Fig. 14, production, grazing and mortality terms are almost zero for the entire season, giving rise to negligibly small net growth and summer diatom biomass. In contrast, primary production of flagellates exceeds the sum of the zooplankton grazing and mortality losses (Fig. 15). The resulting net production therefore keeps the flagellate stocks

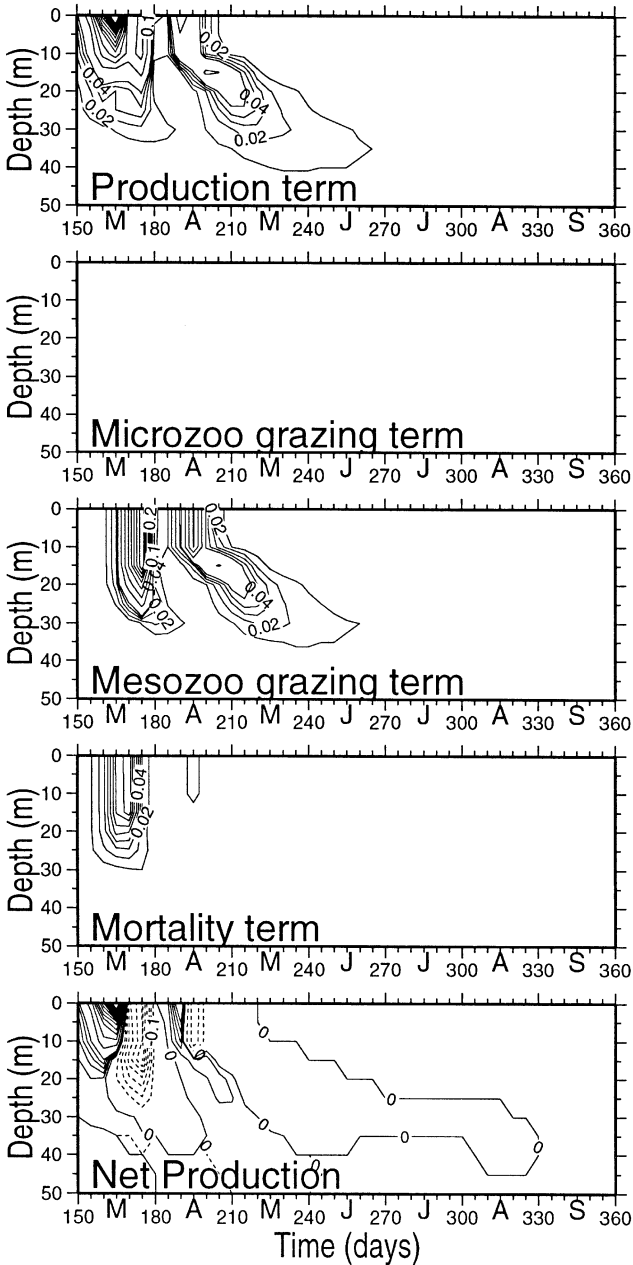


Fig. 14. The depth and time variations of the biological source/sink terms ($\text{mmol N m}^{-3} \text{s}^{-1}$) for the diatom equation. The contour interval is 0.01 for values less than $0.05 \text{ mmol N m}^{-3} \text{s}^{-1}$ and 0.05 for values greater than $0.05 \text{ mmol N m}^{-3} \text{s}^{-1}$. The dash lines represent net production less than zero.

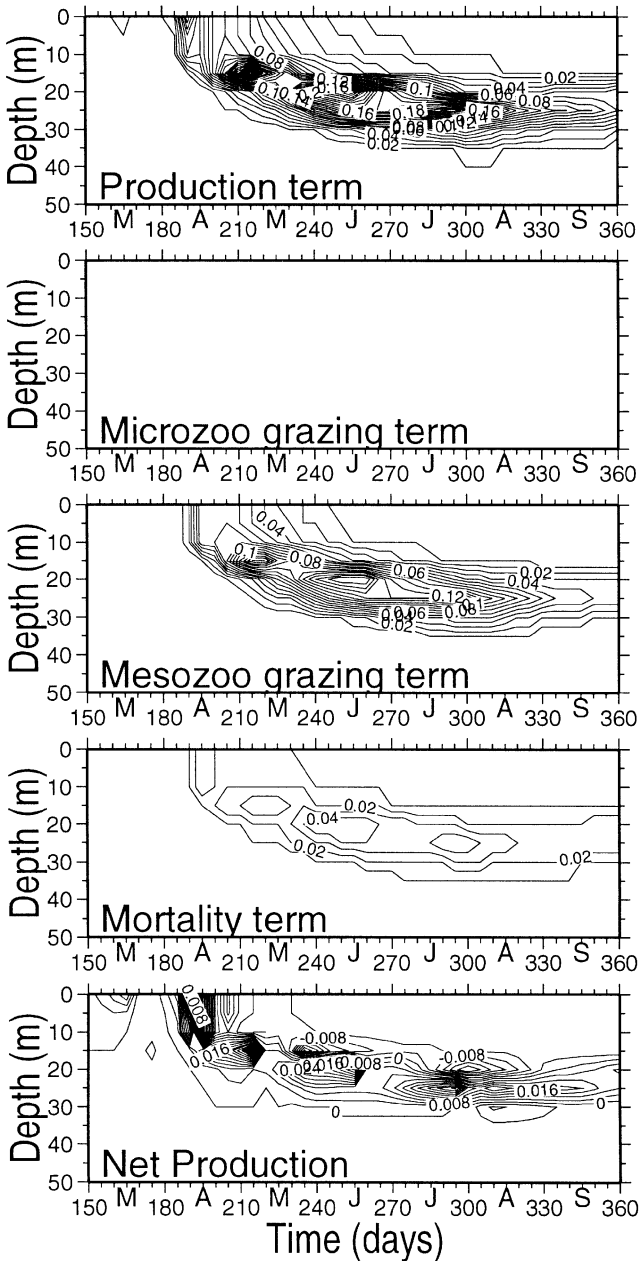


Fig. 15. The depth and time variations of the biological source/sink terms ($\text{mmol N m}^{-3} \text{s}^{-1}$) for the flagellate equation. The contour interval is 0.01 for values less than $0.05 \text{ mmol N m}^{-3} \text{s}^{-1}$ and 0.05 for values greater than $0.05 \text{ mmol N m}^{-3} \text{s}^{-1}$.

above a certain level during the entire summer period. We note that the main grazing pressure for the flagellates is exerted by mesozooplankton. The microzooplankton grazing rate is negligibly small because the entire microzooplankton stock is consumed by the mesozooplankton. Weak grazing control of microzooplankton, however, persists even when the food preference coefficient a_z is reduced from 0.7 to 0.1.

4.7. A simulation with a different formulation of food preferences

Fasham et al. (1990) argued that the assigned preferences in the grazing terms should be expressed as a function of the relative proportion of the food, so that a zooplankton group may have a chance to select the most abundant food group. In this approach, the weighted preferences for microzooplankton are defined by

$$b_k^* = \frac{b_k P_k}{F_s} \quad (17)$$

where the subscript k signifies either f for flagellates or d for diatoms. For mesozooplankton, a similar equation is written

$$a_k^* = \frac{a_k \varphi_k}{F_l} \quad (18)$$

with φ_k representing P_f , or P_d or Z_s . F_s and F_l are given by Eq. (9).

We repeated the experiment described in Section 4.3 (Figs. 8 and 9) by expressing the preferences as in Eqs. (17) and (18) and using the same values of a_k and b_k assigned in Table 1. The resulting phytoplankton distributions are shown in Fig. 16. The differences from the previous simulation are a slight weakening of the autumn bloom and a slight increase in the summer diatom concentrations. The autumn bloom is now dominated by diatoms instead of flagellates. The March and subsequent April diatom blooms remain unchanged. A more important difference between the two simulations is a two-fold reduction in the summer flagellate concentrations. The total (sum of diatom and flagellate) phytoplankton concentrations during the summer months amount to approximately half of the values simulated by the previous case.

In order to evaluate the role of the new preference parameterization on the depth–time distributions of the phytoplankton concentrations and to explain the differences between two simulations, we show in Fig. 17 distributions of the preferences calculated from Eqs. (17) and (18). The most striking feature of these figures is the considerable variation in their values at depths between the seasonal thermocline and the base of the euphotic layer. Due to the depth dependence of the phytoplankton concentrations the food preference coefficients in Eqs. (17) and (18) are subject to considerable vertical variations, which ultimately leads to the differences between the two simulations. We, note however note that the values of preferences within the mixed layer are similar to their prescribed values. These results indicate that a more complex preference formulation might be more appropriate for the mixed layer

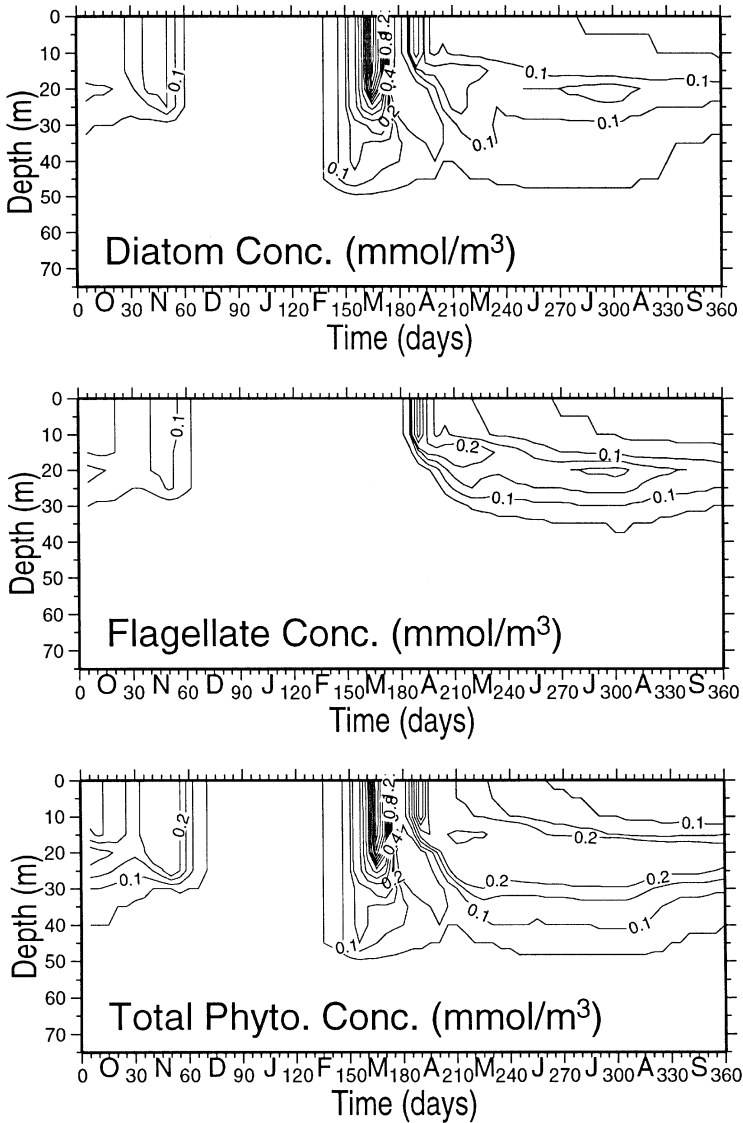


Fig. 16. The model derived annual distributions of (a) diatom biomass, (b) flagellate biomass, and (c) total phytoplankton biomass (mmol N m^{-3}) within the upper layer water column using an alternative formulation of food preference coefficients. The contour interval is 0.05 for phytoplankton biomass values less than $0.2 \text{ mmol N m}^{-3}$ and 0.2 for values greater than $0.2 \text{ mmol N m}^{-3}$.

averaged ecosystem models, but they introduce additional complexity in the vertically resolved models due to their depth dependence. It is, therefore, much more difficult to tune the values of these coefficients in order to obtain realistic model simulations.

4.8. Simulations with oscillatory solutions

A major concern in ecosystem modeling is the oscillation introduced in systems of biological equations. Steele and Henderson (1992) described the way in which higher order mortality functions prevent such oscillations from occurring for the particular set of parameter values in their simplified PZN model. We repeat our simulation experiment to check whether or not a linear zooplankton mortality formulation

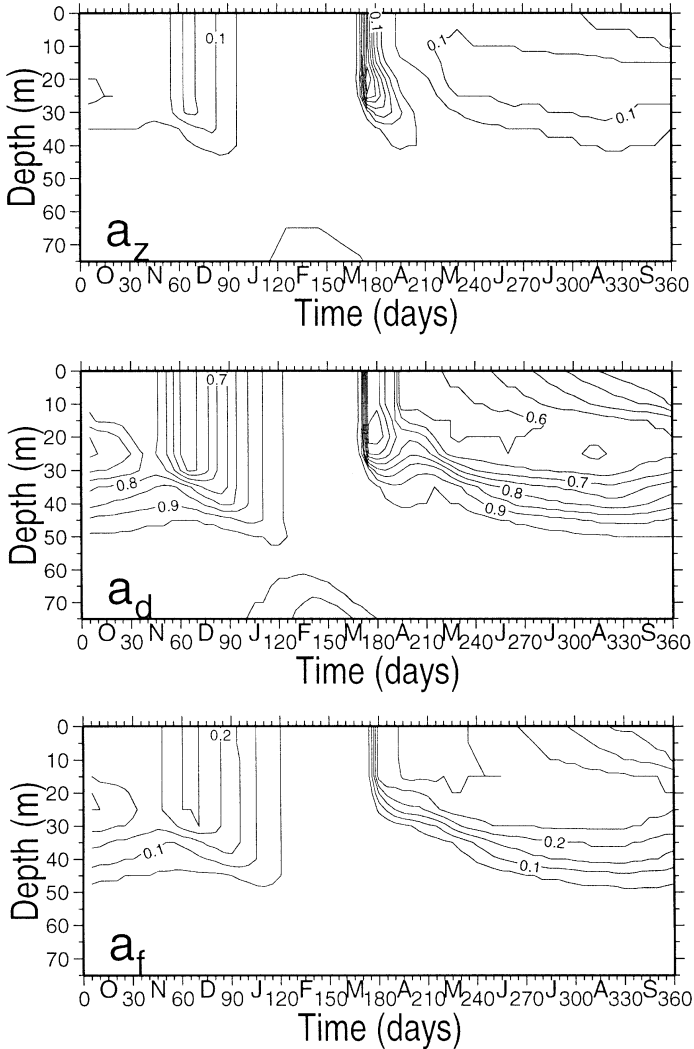


Fig. 17. The annual distributions of the depth and time dependent food preference coefficients computed by Eqs. (17) and (18). The contour interval is 0.05.

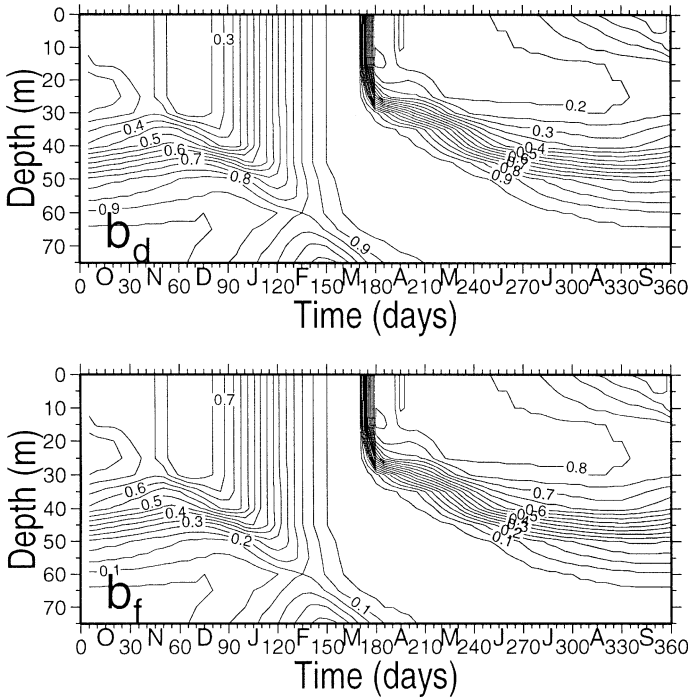


Fig. 17. (continued)

introduces oscillations resulting from predator–prey equation interactions. Using the mortality coefficient of 0.04 d^{-1} (which is half of the coefficient of the quadratic form), the resulting phytoplankton distribution (Fig. 18) has a similar form with comparable phytoplankton biomass distribution during the year. The choice of hyperbolic mortality formulation also leads to similar distributions of phytoplankton and zooplankton. This result implies that the model remains non-oscillatory no matter what type of zooplankton mortality function is specified in the model.

The same is, however, not true when we do not apply grazing on multiple zooplankton and phytoplankton groups as shown in Fig. 1b. We can show this by setting the preference coefficient a_f and b_d to zero in Eqs. (9)–(11), implying a food chain in which flagellates are consumed only by microzooplankton, whereas mesozooplankton eat diatoms and microzooplankton. In this case, both phytoplankton and zooplankton solutions (Fig. 19) exhibit oscillatory character following the March bloom. Similar oscillations also persist when b_d is set to its original value of 0.2, and keeping only $a_f = 0$ (i.e. no flagellate consumption by mesozooplankton). On the other hand, a non-oscillatory solution similar to the one shown in Fig. 9 is obtained when $a_f = 0.3$ (its original value used earlier in our central experiment) and $b_d = 0$ (i.e. no diatom consumption by microzooplankton). These experiments therefore imply that the non-oscillatory solution of the system requires grazing of flagellates by both

Depth Integrated Plankton Biomasses

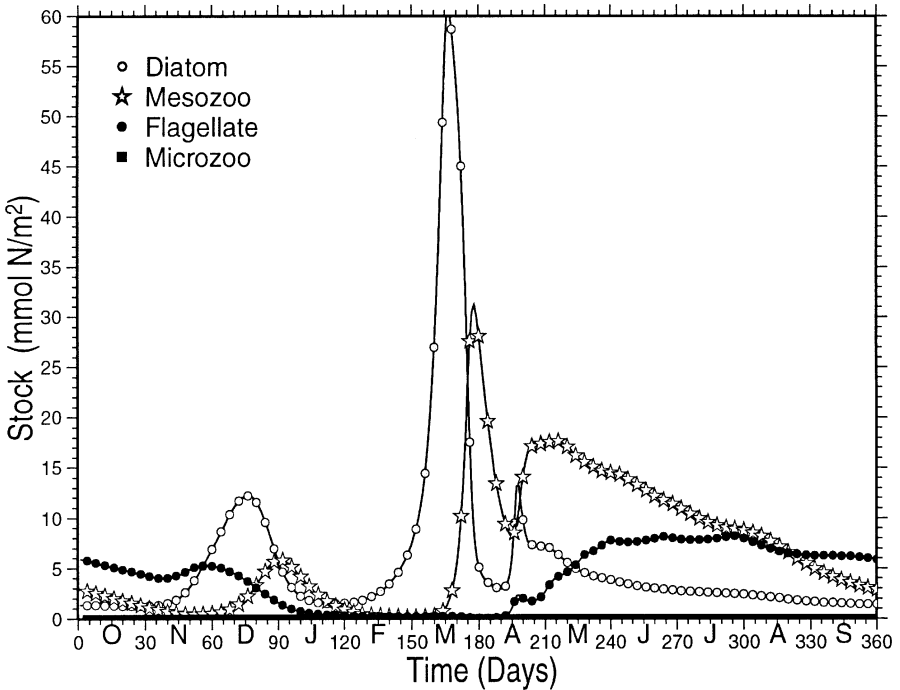


Fig. 18. Annual variations of the euphotic zone integrated plankton biomass (mmol N m^{-2}) computed by the model using the linear zooplankton mortality formulation.

zooplankton groups. Otherwise there will be oscillatory solutions. Only two of the three grazing controls of the mesozooplankton on flagellates, diatoms and microzooplankton are, on the other hand, sufficient to keep the overall solution non-oscillatory.

5. Summary and conclusions

The annual pattern of plankton productivity and nitrogen cycling in the upper water column of the central Black Sea were studied. The work is an extension of the one dimensional, vertically resolved, coupled physical-biochemical model of Oguz et al. (1996) with identical physical characteristics but with a more complex food web structure. Phytoplankton are modeled by two groups, representing diatoms and flagellates. Herbivores are separated into two groups: microzooplankton (nominally $< 200 \mu\text{m}$), consisting of heterotrophic flagellates, ciliates and juvenile copepods; and mesozooplankton ($0.2\text{--}2 \text{ mm}$), consisting essentially of copepods. Both of them feed on two types of prey with different prey capture efficiencies. Microzooplankton are

Depth Integrated Plankton Biomasses

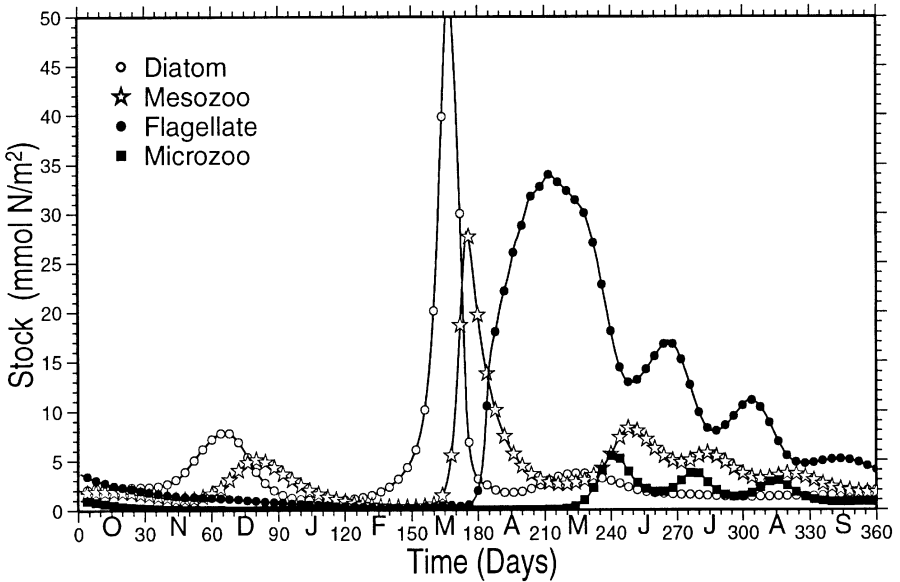


Fig. 19. Annual variations of the euphotic zone integrated plankton biomass (mmol N m^{-2}). Computed by the model with $a_f = b_d = 0$ in Eqs. (9)–(11).

considered to be more efficient at capturing flagellates, whereas diatoms are consumed predominantly by mesozooplankton. We consider that both phytoplankton species groups are limited by a single nutrient (nitrogen) and the same light requirement, even though flagellates withstand higher irradiances than diatoms. Particulate organic material and nutrients (nitrate and ammonium) constitute other components of the biochemical model. The microbial loop has not been incorporated explicitly.

A major finding of this work is to show how a simple size fractionation of the biogenic community structure may lead to increased primary production and development of a more pronounced subsurface chlorophyll maximum layer in the central Black Sea during the summer period.

A diatom-based early spring (March) bloom is followed by summer and autumn blooms of flagellates. They were either absent or had only a weak signature in the previous model of Oguz et al. (1996). The reason for the presence of stronger summer phytoplankton growth in the multi-species/multi-group pelagic food web model may be explained as follows. In the case of single phytoplankton and zooplankton groups, the enhanced grazing pressure exerted on phytoplankton following the March bloom prohibits noticeable phytoplankton development near the base of the euphotic zone during spring and summer (see Fig. 11a–d and Section 4.2.3 in Oguz et al., 1996). In the presence of two phytoplankton and two zooplankton groups, the situation is somewhat different. Diatoms are responsible for the March bloom and support increased mesozooplankton activity later in spring and in summer. As a result of

predator control by mesozooplankton on their grazers, flagellates do not experience any grazing pressure from the microzooplankton and may therefore provide a stronger subsurface production during the summer. This result implies that the choice of a 1P1Z model (together with nutrients and detritus) may not be entirely adequate for representation of all bloom events within a year.

The second major feature of the model is its ability to reproduce a fairly realistic nutrient recycling mechanism. Dead cells and fecal matter sinking from the euphotic zone are continually remineralized to ammonium, which is subsequently oxidized to nitrate. These conversion processes are accompanied at the same time by upward transport of both nitrate and ammonium to supply them back to the surface waters. The model simulations indicate that a major part of this recycling takes place within the upper 50 m of the water column. Nearly 90% of the primary production is recycled there. The annual nitrogen budget for the euphotic zone shows that 60% of the primary production is supported by the ammonium resources recycled within the euphotic zone. About 15% of the nitrate-based production constitutes new production, whereas the rest originates from recycled nitrate within the euphotic layer as a result of the remineralization–ammonification–nitrification pathway. The remaining remineralization–nitrification occurs within the oxycline–nutricline zone, confined between the euphotic zone and the suboxic layer (50–75 m). This gives rise to gradually increasing nitrate concentrations from the near-surface to the upper boundary of the suboxic zone, where the nitrate maximum occurs, with concentrations of $8.0 \text{ mmol N m}^{-3}$ at approximately 75 m.

Steele and Henderson (1992) pointed out the significance of the form of mortality closure in simple PNZ models. It was shown that the limit cycle solution obtained in the case of linear zooplankton mortality might be avoided by using higher order (parabolic or hyperbolic, etc.) functions. In our more sophisticated ecosystem model, all kinds of zooplankton mortality formulations provide stable solutions with similar annual variations of phyto- and zooplankton when the mortality parameters are adjusted for each case. We think that complicated forms of nutrient limitation and grazing controls together with vertical diffusion terms prevent limit cycle behaviour of the system. On the other hand, the ecosystem is shown to possess an oscillatory character when flagellates are not grazed by both zooplankton groups. This is demonstrated by an example in which flagellates are ingested only by microzooplankton.

In the model, we explored the feasibility of using two different types of food preference formulations. Assigning constant values for the coefficients of food capturing efficiencies turns out to be more practical for obtaining realistic model simulations in the vertically resolved models. The weighted preference formulation, on the other hand, introduces depth and time dependencies on these coefficients which generate additional complexity in the model simulations.

Acknowledgements

We wish to thank M.E. Vinogradov and L.P. Lebedeva for many discussions. This work was carried out within the scope of the TU-Black Sea Project sponsored by the

NATO Science for Stability Program. It was supported partially by the Turkish Scientific and Technical Research Council (TUBITAK), the Office of Naval Research Grant No. N000 14-95-1-0226 and NSF Grant OCE-9633145. Under these grants, T. Oguz was a visiting scientist at MIT during June–August of 1995 and 1996. H. Ducklow was supported by NSF Grant OCE-9633145. J. Murray was supported by NSF Grant OCE 9633571.

References

- Armstrong, R.A., 1994. Grazing limitation and nutrient limitation in marine ecosystems: steady state solutions of an ecosystem model with multiple food chains. *Limnology and Oceanography* 39, 597–608.
- Basturk, O., Saydam, C., Salihoglu, I., Eremeeva, L.V., Konovalov, S.K., Stoyanov, A., Dimitrov, A., Cociasu, A., Dorogan, L., Altabet, M., 1994. Vertical variations in the principle chemical properties of the Black Sea in the autumn of 1991. *Journal of Marine Chemistry* 45, 149–165.
- Bologa, A.S., 1986. Planktonic primary productivity of the Black Sea: a review. *Thalassia Yugoslavia* 21/22, 1–22.
- Boudreau, B.P., Leblond, P.H., 1989. A simple evolutionary model for water and salt in the Black Sea. *Paleoceanography* 4, 157–166.
- Brewer, P.G., Murray, J.W., 1973. Carbon, nitrogen and phosphorus in the Black Sea. *Deep Sea Research* 20, 803–818.
- Burlakova, Z.P., Eremeeva, L.V., Konovalov, S.K., 1997. Particulate organic matter of Black Sea euphotic zone: seasonal and long-term variation of spatial distribution and composition. In: Ozsoy, E., Mikaelyan, A. (Eds.), *Sensitivity to Change: Black Sea, Baltic Sea and North Sea*, NATO ASI Series 2: Environment, vol. 27, pp. 223–238.
- Coban, Y., 1997. The abundance and elemental composition of suspended organic matter in the Turkish (Black, Marmara and Eastern Mediterranean) Seas. M.Sc. Thesis. Institute of Marine Sciences, Middle East Technical University.
- Codispoti, L.A., Friederich, G.E., Murray, J.W., Sakamoto, C.M., 1991. Chemical variability in the Black Sea: implications of continuous vertical profiles that penetrated the oxic/anoxic interface. *Deep Sea Research* 38 (Suppl. 2), S691–S710.
- Deuser, W.G., 1971. Organic-carbon budget of the Black Sea. *Deep Sea Research* 18, 995–1004.
- Doney, S.C., Glover, D.M., Najjar, R.G., 1996. A new coupled, one-dimensional biological-physical model for the upper Ocean: applications to the JGOFS Bermuda Atlantic Time-Series Study (BATS) site. *Deep Sea Research II* 43, 591–624.
- Ducklow, H.W., Fasham, M.J.R., 1992. Bacteria in the greenhouse: modelling the role of oceanic plankton in the global carbon cycle. *Environmental Microbiology*. Wiley-Liss Inc, New York, pp. 1–31.
- Dugdale, R.G., Goring, J.J., 1967. Uptake of new and regenerated forms of nitrogen in primary production. *Limnology and Oceanography* 12, 196–206.
- Fasham, M.J.R., Ducklow, H.W., McKelvie, S.M., 1990. A nitrogen-based model of plankton dynamics in the oceanic mixed layer. *Journal of Marine Research* 48, 591–639.
- Finenko, Z.Z., 1979. Principles of the biological productivity of the Black Sea. *Naukova Dumka*, Kiev, pp. 88–89 (in Russian).
- Gargett, A.E., 1984. Vertical eddy diffusivity in the ocean interior. *Journal of Marine Research* 42, 359–393.
- GLOBEC, 1995. Report of working Group 1, Critical variables and dominant scales, Globec Numerical Modeling Group Meeting, Nantes, 17–20 July 1995.
- Hurtt, C.H., Armstrong, R.A. 1996. A pelagic ecosystem model calibrated with BATS data. *Deep Sea Research II* 43, 653–683.
- Jamart, B.M., Winter, D.F., Banse, K., Andeson, G.C., Lam, R.K., 1997. A theoretical study of phytoplankton growth and nutrient distribution in the Pacific Ocean off the northwestern US coast. *Deep Sea Research* 24, 752–773.

- Jasby, A.D., Platt, R., 1976. Mathematical formulation of the relationship between photosynthesis and light for phytoplankton. *Limnology and Oceanography* 21, 540–547.
- Karl, D.M., Knauer, G.A., 1991. Microbial production and particle flux in the upper 350 m of the Black Sea. *Deep Sea Research* 38 (Suppl. 2), S655–S661.
- Klein, P., Coste, B., 1984. Effects of wind-stress variability on nutrient transport into the mixed layer. *Deep Sea Research* 31, 21–37.
- Koblentz-Mishke, O.J., Volkovinsky, V.V., Kabanova, J.G., 1970. Plankton primary production of the world ocean. In: Wooster, W.S. (Ed.), *Scientific Exploration of the South Pacific*. National Academy of Sciences, Washington, pp. 183–193.
- Lebedeva, L.P., Vostokov, S.V., 1984. Studies of detritus formation processes in the Black Sea. *Oceanology* 24, 258–263.
- Lewis, B.L., Landing, W.M., 1991. The biogeochemistry of manganese and iron in the Black Sea. *Deep Sea Research* 38 (Suppl. 2), S773–S803.
- Longhurst, A., 1995. Seasonal cycles of pelagic production and consumption. *Progress in Oceanography*, 36, 77–167.
- Loukos, H., Frost, B., Harrison, E., Murray, J.W., 1997. An ecosystem model with iron limitation of primary production in the equatorial Pacific at 140°W. *Deep Sea Research II* 44, 2221–2250.
- Murray, J.W., Jannash, H.W., Honjo, S., Anderson, R.F., Reeburgh, W.S., Top, Z., Friederich, G.E., Codispoti, L.A., Izdar, E., 1989. Unexpected changes in the oxic/anoxic interface in the Black Sea. *Nature* 338, 411–413.
- Murray, J.W., Codispoti, L.A., Friederich, G.E., 1995. Oxidation-reduction environments: the suboxic zone in the Black Sea. In: Huang, C.P., O'Melia, C.R., Morgan, J.J. (Eds.), *Aquatic Chemistry: Interfacial and Interspecies Processes*. ACS Advances in Chemistry Series, vol. 244, pp. 157–176.
- Murray, J.W., Lee, B.S., Bullister, J., Luther III, G.W., 1999. The Suboxic Zone of the Black Sea. *Proc. NATO Advanced Research Workshop Environmental Degradation of the Black Sea: Challenges and Remedies*, Constantza, Romania, 6–10 October 1997, to appear.
- Oguz, T., La Violette, P.E., Unluata, U., 1992. The Black Sea circulation: its variability as inferred from hydrographic and satellite observations. *Journal of Geophysical Research* 97, 12569–12584.
- Oguz, T., Ducklow, H., Malanotte-Rizzoli, P., Tugrul, S., Nezhin, N.P., Unluata, U., 1996. Simulation of annual plankton productivity cycle in the Black Sea by a one-dimensional physical–biological model. *Journal of Geophysical Research* 101, 16585–16599.
- Oguz, T., Malanotte-Rizzoli, P., Ducklow, H.W., 1997. Towards coupling a three dimensional general circulation model with a biochemical model of nutrient cycling and bacteria-plankton dynamics in the Black Sea. In: Ozsoy, E., Mikaelyan, A. (Eds.), *Sensitivity of North Sea, Baltic Sea and Black Sea to Anthropogenic and Climatic Changes*. NATO ASI Series. Kluwer Academic Publishers, The Netherlands, pp. 469–486.
- Prunet, P., Minister, J.F., Pino, D.R., Dadou, I., 1996. Assimilation of surface data in a one-dimensional physical–biogeochemical model of the surface ocean: 1. Method and preliminary results. *Global Biogeochemical Cycles* 10, 111–138.
- Sarmiento, J.L., Slatter, R.D., Fasham, M.J.R., Ducklow, H.W., Toggweiler, J.R., Evans, G.T., 1993. A seasonal three-dimensional ecosystem model of nitrogen cycling in the North Atlantic euphotic zone. *Global Biogeochemical Cycles* 7, 417–450.
- Sorokin, Yu. I., 1983. The Black Sea. In: Ketchum, B.H. (Ed.), *Estuaries and Enclosed Seas. Ecosystem of the World*. Elsevier, New York, pp. 253–292.
- Steele, J.H., Henderson, E.W., 1992. The role of predation in plankton models. *Journal of Plankton Research* 14, 157–172.
- Stigebrandt, A., Wulff, F., 1987. A model for the dynamics of nutrients and oxygen in the Baltic proper. *Journal of Marine Research* 45, 729–759.
- Sur, H.I., Ozsoy, E., Ilyin, Y.P., Unluata, U., 1996. Coastal/deep ocean interactions in the Black Sea and their ecological/environmental impacts. *Journal of Marine Systems* 7, 293–320.
- Vedernikov, V.I., Demidov, A.B., 1993. Primary production and chlorophyll in the deep regions of the Black Sea. *Oceanology* 33, 193–199.

- Vidal, C.V., 1995. Bio-optical characteristics of the Mediterranean and the Black Sea. M.Sc. Thesis, Institute of Marine Sciences, Middle East Technical University, Turkey.
- Vinogradov, M.E., 1992. Long-term variability of the pelagic community structure in the open Black Sea. Paper presented at the Problems of Black Sea Int. Conf., Sevastopol, Ukraine, 10–15 November, 1992.
- Ward, B.B., Kilpatrick, K.A., 1991. Nitrogen transformations in the oxic layer of permanent anoxic basins: the Black Sea and Cariaco Trench. In: Izdar, E., Murray, J.W. (Eds.), *Black Sea Oceanography*. NATO ASI Series C, vol. 351. Kluwer Academic Publishers, Dordrecht, pp. 111–124.